

Systematic behavior of the fusion barrier parameters for heavy ion pairs

By

Abdulghany Reda Abdulghany Ahmed

**A Thesis Submitted to
Faculty of Science**

**In Partial Fulfillment of the Requirements for the degree of
Master of Science
(Theoretical physics)**

**Physics Department
Faculty of Science
Cairo University**

(2010)

APPROVAL SHEET FOR SUBMISSION

Thesis Title

Systematic behavior of the fusion barrier parameters for heavy ion pairs

Name of candidate

Abdulghany Reda Abdulghany Ahmed

This thesis has been approved for submission by the supervisors:

1- Prof. Dr. Mahmoud Yahia Ismail

Physics Department - Faculty of Science - Cairo University

Signature:

2- Dr. Ali Yahia Ellithi

Physics Department - Faculty of Science- Cairo University

Signature:

Prof. Dr. Gamal Abd-Elnaser Madbouly

Chairman of Physics Department

Faculty of Science - Cairo University

Signature:

ABSTRACT

The nucleus-nucleus potential is calculated in the frame work of the double folding model (DFM) to obtain the Coulomb barrier parameters (barrier position and height), starting from M3Y-Reid nucleon-nucleon interaction and realistic nuclear matter distribution. The systematic behavior of the barrier parameters with mass numbers, charges, and radii of interacting nuclei is studied. The relation between the barrier height and radius is also discussed. The systematic behavior of the barrier parameters is presented in the form of simple analytical formulae, which can be used to calculate the barrier position and height directly, and show which factors can affect them.

The potentials obtained from DFM are used to derive a universal function of the nuclear proximity potential which is useful for barrier calculations for heavy ion reactions. The obtained universal function reproduces the barrier parameters within less than 2% deviation from the values obtained using DFM for heavy and super heavy ion reactions. Reactions involving α -particle are studied individually, and another form of the universal function is presented.

Acknowledgements

First of all, I would like to thank my supervisor Prof. Dr. Mahmoud Yahia Ismail, who guided me to complete successfully my thesis, and who also have kindly and meticulously undertaken the tedious work of proofreading my thesis, I would express my appreciation to him not only for his professional advice and guidance, but also for his enthusiasm and encouragement. I would also like to thank Dr. Ali Yahia Ellithi, my second supervisor, who helped me on my simulation work, and whose comments and questions have helped me deepen my understanding about many parts of the research.

I am indebted to many of my colleagues, who helped me through the year by their friendships and by giving helpful comments, and supported me all the time.

I would also like to express my gratitude to my wife Marwa, without her support, this thesis would have never come to completion.

Abdulghuny, 2010.

Table of Contents

List of Tables	vi
List of Figures.....	vii
Preface.....	x
Chapter 1 Systematic behavior of the fusion barrier parameters using the double folding model	1
1.1 Introduction	1
1.2 Double folding model (DFM).....	7
1.3 Details of calculation	10
1.4 Numerical calculations and results	14
1.5 Discussion.....	36
References.....	44
Chapter 2 Universal function of nuclear proximity potential derived from M3Y nucleon-nucleon interaction.....	48
2.1 Introduction.....	48
2.2 Calculation of universal function starting from M3Y-Reid NN interaction	54
2.3 Discussion.....	67
References.....	75
Appendix 1 DFM and Fourier transformation.....	77
Appendix 2 Units of Coulomb constant.....	85

List of Tables

Table 1.1: Density-distribution parameters obtained from elastic electron scattering.....	14
Table 1.2- <i>a</i> : Barrier position (R_B), barrier height (V_B), Coulomb interaction at $R=R_B$ (V_C), and nuclear interaction at $R=R_B$ (V_N), for the reactions between different targets and ${}^4\text{He}$ as projectile.....	16
Table 1.2- <i>b</i> : The same as Table (1.2- <i>a</i>) but for ${}^{16}\text{O}$ projectile..	17
Table 1.2- <i>c</i> : The same as Table (1.2- <i>a</i>) but for ${}^{40}\text{Ca}$ projectile.....	18
Table 1.2- <i>d</i> : The same as Table (1.2- <i>a</i>) but for ${}^{60}\text{Ni}$ projectile..	19

List of Figures

Figure 1.1: Coordinates used in the double folding model	8
Figure 1.2-a: The variation of calculated barrier position (R_B) with $\langle r_T^2 \rangle^{1/2} + \langle r_P^2 \rangle^{1/2}$ for the reactions with ${}^4\text{He}$	20
Figure 1.2-b: The same as Figure (1.2-a) but for ${}^{16}\text{O}$ as projectile.....	21
Figure 1.2-c: The same as Figure (1.2-a) but for ${}^{40}\text{Ca}$ as projectile.....	22
Figure 1.2-d: The same as Figure (1.2-a) but for ${}^{60}\text{Ni}$ as projectile.....	23
Figure 1.3-a: The differences between the values of R_B calculated using DFM analysis and the values calculated using the formula (1.12).....	24
Figure 1.3-b: The differences between the values of R_B calculated using DFM analysis and the values calculated using the analytical formula obtained for reactions with ${}^4\text{He}$	25
Figure 1.4-a: The variation of calculated barrier height (V_B) with $Z_T Z_P / (A_T^{1/3} + A_P^{1/3})$ for the reaction with ${}^4\text{He}$	26
Figure 1.4-b: The same as Figure (1.4-a) but for ${}^{16}\text{O}$ as projectile.....	27
Figure 1.4-c: The same as Figure (1.4-a) but for ${}^{40}\text{Ca}$ as projectile.....	28
Figure 1.4-d: The same as Figure (1.4-a) but for ${}^{60}\text{Ni}$ as projectile.....	29
Figure 1.5-a: The variation of calculated barrier height (V_B) with $(Z_T Z_P / R_B)$ for the reaction with ${}^4\text{He}$	30
Figure 1.5-b: The same as Figure (1.5-a) but for ${}^{16}\text{O}$ as projectile.....	31
Figure 1.5-c: The same as Figure (1.5-a) but for ${}^{40}\text{Ca}$ as projectile.....	32
Figure 1.5-d: The same as Figure (1.5-a) but for ${}^{60}\text{Ni}$ as projectile.....	33
Figure 1.6-a: The behavior of $(R_B V_B)$ product for all reaction done in chapter (1) with $Z_T Z_P$	34

Figure 1.6- <i>b</i> : the relative differences in the values of $R_B V_B$ calculated using DFM and the values calculated using formula (1.13) for all reactions studied in chapter (1).....	35
Figure 2.1: the minimum separation distance (ξ_0) between the nuclear surfaces for interaction between two spherical nuclei	51
Figure 2.2- <i>a</i> : Universal function $\Phi(s_0)$ calculated from DFM with M3Y interaction as a function of the dimensionless separation s_0 , for symmetric reactions between ions of mass numbers up to 238.	58
Figure 2.2- <i>b</i> : The same as Figure (2.2- <i>a</i>) but with s_0 varying in the range [-1, 4].....	59
Figure 1.3- <i>a</i> : Calculated universal function $\Phi(s_0)$ as a function of the dimensionless separation s_0 , for reactions involve ions of mass numbers up to 50, and surface diffuseness between 0.9 and 1.1.....	60
Figure 1.3- <i>b</i> : The same as Figure (2.3- <i>a</i>) but for reactions involve ions of mass numbers A as: $50 > A > 238$. Different shapes of the universal function are plotted	61
Figure 2.4- <i>a</i> : Fractional error between the values of potential barrier position calculated using the proximity model with universal function given by formula (2.9), and values calculated using DFM, for reactions between ^{63}Cu and different ions.....	62
Figure 2.4- <i>b</i> : Fractional error between the values of potential barrier height calculated using the proximity model with universal function given by formula (2.9), and values calculated using DFM, for reactions between ^{63}Cu and different ions.....	63

Figure 2.5- <i>a</i> : Calculated universal function $\Phi(s_0)$ as a function of the dimensionless separation s_0 , for reactions between ${}^4\text{He}$ and target nuclei with mass numbers up to 238.....	64
Figure 2.5- <i>b</i> : Same as Figure (2.5- <i>a</i>), but for target nuclei of mass numbers A as, $50 > A > 238$. The solid line is the universal function derived from the best fit to data, given by formula (2.10).....	65
Figure 2.5- <i>c</i> : Same as Figure (2.5- <i>b</i>), but s_0 range varying in the range $[-10, 6]$	66

Preface

In the last few decades, the study of nuclear reactions became one of the most interesting fields of physics. The main focus was on production of energy; however, nuclear studies affect many vital fields, such like medicine, biology, archeology and militarism. As the building of accelerators developed the scientific ambition developed, and many studies were performed on the synthesis of new super heavy elements (SHE). This opened up a new field of research termed as heavy-ion collision physics. Most of our information is obtained from studies made on stable nuclei for the simple reason that they are far easier to handle in the laboratory. This is a very special group among all the possible ones that can be formed. Synthesis of SHE is a great challenging topic, not to get the SHE itself, but to get a detailed picture about the shell stabilization and structure effects. This also gives a new tool to test the nuclear theories, or even develop them.

The building blocks of nuclei are neutrons and protons, two quantum states of the same particle, the nucleon. Both gravitational and electromagnetic forces are infinite in range and their interaction strengths diminish with the square of the distance of separation. Clearly, nuclear force cannot follow the same radial dependence. The nuclear force has a very short range, not much beyond the confine of the nucleus itself. In 1935, Yukawa proposed that the force between nucleons arises from meson exchange. This was the start of the concept of field quantum as the mediator of fundamental forces. The reason that nuclear force has a finite range comes from the nonzero rest mass of the mesons exchanged. For the nucleons

inside a nucleus, nuclear force is far stronger than that due to electromagnetic interaction. This force keeps the protons and the neutrons bound to the nucleus, and it makes the nuclear reactions possible.

The interaction between two nuclei is governed by the repulsive Coulomb potential and the attractive nuclear potential, which in combination form the potential barrier; this barrier has to be penetrated for fusion to occur. Understanding the physics of fusion of heavy ions is still a central topic of research in nuclear physics. For this purpose many studies of fusion barrier have been done. Well knowledge of fusion barrier parameters (barrier height and barrier position) gives a great idea about the process of fusion and tells us about the conditions needed to get the wanted result. In chapter (1) of the present thesis we review the effect of different factors such like, masses, charges, diffuseness of nuclear matter, and radii of the interacting pair on the barrier parameters. We introduce the behavior of the fusion barrier parameters in the form of simple analytical formulae, not only to get a simple method to predict the values of barrier parameters, but also to show which factors can affect them. In chapter (2) we introduce a method to calculate nuclear potential around the barrier position. We use the advantages of two different models, the first is the “double folding model” which characterized by its great validity in the tail region (around the barrier position), and the second is the “proximity model” which characterized by the accessibility in the calculation of nuclear interaction. We used the results of detailed calculations through the double folding model to introduce a new shape of the universal function useful in barrier calculations for heavy ion reactions. We also study the reactions involve α -particle individually,

because of its odd characteristics, and we introduce a universal function useful for reactions involve α -particle and α -decay.

Chapter 1

*Systematic behavior of the fusion barrier
parameters using the double folding model*

Chapter 1

Systematic behavior of the fusion barrier parameters using the double folding model

1.1 Introduction

The interaction between two nuclei is governed by two potentials, the first is the repulsive Coulomb potential and the second is the attractive nuclear potential. The combination between these potentials forms the potential barrier; this barrier has to be penetrated for fusion to occur. The nucleus-nucleus potential [1- 3] plays an important role in the description of fusion in any model [3-7]. Coulomb interaction is well known from the classical treatment of the electrostatic force between charged bodies, but the nuclear contribution of the interaction potential is less known. For many studies of nucleon and light ion scattering, the major part of the nuclear interaction potential can be approximated by a Woods-Saxon (WS) form [8-11] which gives a simple analytic expression. The WS real potential combined with an imaginary part of the same radial shape, or

slightly modified shape, forms the optical model potential [12-16]. This potential has been used successfully for the scattering of light ions.

Historically, the basis of the optical model was developed by comparing the results of the scattering of neutrons by nuclei to those obtained in optics for the scattering of light by transparent spheres. The first optical potentials were built for the interaction of neutrons with nuclei and afterwards for the scattering of protons [17, 18], α - particles [19] and heavy ions [5, 20-22]. The optical potential consists of two parts; the first part is a real part and it deals with the refraction, the second is an imaginary part and it deals with the absorption into reaction channels.

The interaction between heavy ions (HI) may be quite complicated; however, if we are only interested in the averaged properties, it is possible to simplify the situation by a large extent. An optical model potential for interaction between target and projectile can represent the average interaction between the incident nucleons in the projectile nucleus and nucleons in the target nucleus. It, therefore, replaces the complicated many body problem posed by the interaction of two nuclei by the much simpler problem of two particles interacting through a potential. A microscopic model of the potential may be constructed by folding the fundamental nucleon-nucleon interaction with the nuclear

densities [5]. Such a folding model has been known to be quite successful in describing nucleus-nucleus interaction [5, 23, 24] data if an appropriate nucleon-nucleon interaction is used as the starting point.

Recently, the double folding model (DFM) plays an important role in the description of nuclear reactions. The DFM, which starts from realistic nuclear densities, has become one of the most popular methods for calculating the real part of the optical potential. On the basis of the DFM, detailed fits to elastic-scattering data for many systems were obtained [5, 23, 25-28], and helped in developing phenomenological potentials [23,27,31,32] to give good agreement with data.

The different nuclear density distributions can be introduced in the folding calculation. The average nuclear matter density is somewhat smaller than the density at the center of the nucleus (ρ_0). This is attributed to a large diffused surface region where the density drops off to zero more or less exponentially. The nuclear densities can be obtained for example from Hartree-Fock Boglioubov calculations [33, 34] or from a Quasiparticle Random Phase Approximation with Skyrme's forces [33, 35]. For many purposes, the radial distribution of nuclear density may be represented by two-parameter Fermi (2pF) distribution or three-parameter Fermi (3pF) distribution. Information about the nuclear density may be

obtained from electron scattering measurements. These give directly the charge distribution from which proton distribution may be obtained. Parameters for different density distributions are calculated for the most of nuclei. In the present thesis, the tabulated parameters in reference [36] are used for the proton density with 2pF and 3pF distributions, they are given in table (1.1). Total nucleon distribution is approximated to have the same radial distribution as the proton distribution with magnitude ratio of A/Z .

Nucleus-nucleus potential is a function of center of mass separation distance (R) between the two interacting nuclei. At large separation, where the hadronic forces have become negligible, the heavy ion (HI) potential between two spherical nuclei become pure Coulomb interaction, which usually assumed to be clear and equal to

$$U_c(R) = \frac{k_e Z_1 e \times Z_2 e}{R}$$

The R^{-1} dependence of $U_c(R)$ is no longer valid when the two nuclear surfaces begin to overlap at smaller values of R . Frequently, the Coulomb potential at small R is represented by the potential felt by a point charge incident upon a charge distribution. The correct way to calculate the HI Coulomb potential is through the DFM; folding the

charge density distributions with the proton-proton Coulomb potential $v_c(r_{12})$ can efficiently be used to calculate $U_c(R)$ for any separation distance R [5],

$$v_c(r_{12}) = \frac{k_e e^2}{r_{12}},$$

Thus the Coulomb potential between two nuclei can be calculated efficiently by double folding model [37], but the calculation of nuclear potential is more difficult to be done [5, 21, 22, 38] due to the lack of knowledge of the effective nucleon-nucleon hadronic interaction, and the mathematical complications of the many body problem. Recently many trials have been made to simplify the effective nucleon-nucleon interaction; but that which became known as M3Y [39] is probably the most widely used and certainly is representative of realistic interactions. Two versions of M3Y interaction namely, M3Y-Reid [40] and M3Y-Paris [41] effective interactions were later developed. The effective interaction depends on energy, momentum, spin, isospin and nucleons density distribution [42, 43]. Therefore, M3Y nucleon-nucleon force may have many approximate shapes as these effects are involved or not [23]. An exchange part (zero-range or finite-range) may be added to M3Y interactions [44- 46]. These M3Y interactions are purely real, so that the

imaginary part of the optical potential either has to be constructed independently or, most frequently, treated phenomenologically [47].

Fusion barrier is a very important quantity in the field of super heavy elements (SHE) study. The values of barrier parameters are needed to choose the optimum conditions for SHE synthesis, and show how it is possible to be stable or decay [48-50]. Calculation of fusion-barrier is a main milestone of the present chapter. Fusion-barrier appears in the net interaction potential between two nuclei, which is the sum of all interactions. Nuclear potential has too short range compared to Coulomb potential so; the net interaction potential is positive (repulsive) at large values of (R). As the two nuclei become closer the total potential increases till reaches its maximum value (V_B) at distance (R_B), then it decreases rapidly to negative values when the interacting pair fuses forming a bound system of nucleons. Height of the barrier is expected to be proportional to Z_1Z_2 , which stands from the classical definition of coulomb potential [51]. The behavior of barrier height for different interacting pairs may deviate from the well defined proportionality relation, mentioned above, for one or more reason, which will be discussed within the present chapter. The radius of the potential barrier is also expected to increase as the sum of interacting pair radii (R_1+R_2).

Detailed study of the potential barrier parameters will be performed in the present chapter to understand their dependence on the entrance channel of the fusion reaction.

The aim of the present chapter is to study the systematic behavior of the fusion barrier parameters for large number of interacting ion pairs and its dependence on the composition of the interacting nuclei looking for simple and direct analytical expression for calculation of the interaction barrier starting from masses, charges, and radii of interacting nuclei. DFM will be used to derive the interaction potential, starting from empirical nuclear density and M3Y nucleon-nucleon force, which will be represented briefly in the next sections.

1.2 Double folding model (DFM)

It is generally assumed that the interaction $U(\mathbf{R})$ is a sum of local two-body potential $v(r_{12})$, although many-body aspects may be represented by a dependence of $v(r_{12})$ on the density of the nuclear matter in which the two interacting nucleons are embedded [5]. Then the folded potential may be written as

$$U(\mathbf{R}) = \int d\mathbf{r}_1 \int d\mathbf{r}_2 \rho_1(\mathbf{r}_1) v(\mathbf{r}_{12}) \rho_2(\mathbf{r}_2) \quad (1.1)$$

$$r_{12} = |\mathbf{R} + \mathbf{r}_2 - \mathbf{r}_1|$$

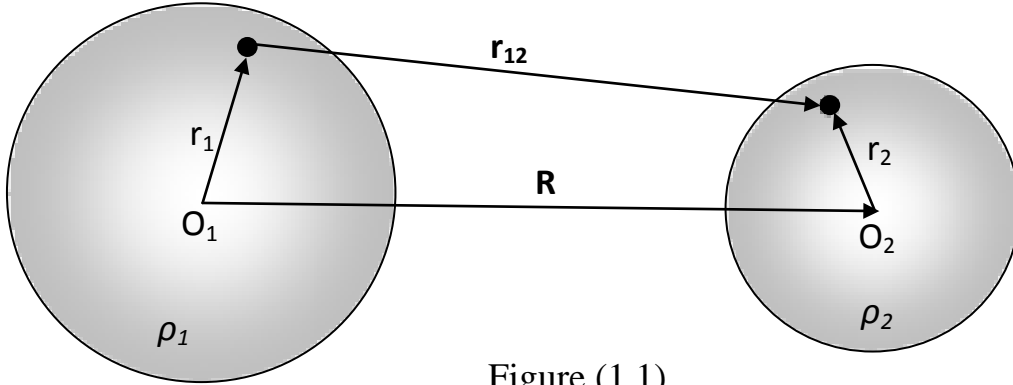


Figure (1.1)

The coordinates are defined in Figure (1.1), where R is the distance between the mass centers of the two interacting nuclei. Here $\rho_1(\mathbf{r}_1)$ and $\rho_2(\mathbf{r}_2)$ are the density distributions of the projectile and target ground states respectively, normalized so that

$$\int \rho_i(\mathbf{r}) d\mathbf{r} = X_i \quad , (i = 1,2) \quad (1.2)$$

where X is the number of nucleons which are sensitive for the interaction $v(r_{12})$, i.e. X is the number of protons for Coulomb interaction, and the mass number for nuclear interaction. For a scalar potential $v(r_{12})$ and if density distributions of both nuclei are taken to be spherically symmetric, then the folded potential $U(\mathbf{R})$ is spherically symmetric; if one or both densities are nonspherical, $U(\mathbf{R})$ will be nonspherical.

The calculation of nucleus-nucleus interaction using the double folding model, given by equation (1.1), includes complicated integrations and is not easy to evaluate, but it becomes easy to calculate if we work in momentum space [5,52]; the double folding reduces to a product of three Fourier transforms; see (appendix 1-A). Often the Fourier transform of the effective nucleon-nucleon potential $v(r_{12})$ has an analytic form and need not to be done numerically; see (appendix 1-B).

From the convolution theorem the Fourier transform of the folded quantity is simply the product of the transforms of the individual component functions. This makes the calculation much easier than directly doing the folding integrals

$$\tilde{U}(\mathbf{k}) = \tilde{\rho}_1(\mathbf{k})\tilde{v}(\mathbf{k})\tilde{\rho}_2(-\mathbf{k}) \quad (1.3)$$

If the density distribution is spherically symmetric, we can apply the simplified expression of Fourier transform by integrating over the solid angle to get,

$$\tilde{\rho}(k) = 4\pi \int j_0(kr) \rho(r) r^2 dr \quad (1.4)$$

So that

$$\tilde{U}(\mathbf{k}) = \left[4\pi \int j_0(kr_1) \rho_1(r_1) r_1^2 dr_1 \right] \tilde{v}(\mathbf{k}) \left[4\pi \int j_0(kr_2) \rho_2(r_2) r_2^2 dr_2 \right] \quad (1.5)$$

The potential $\tilde{v}(k)$ has an analytic form, and each of the two square brackets in equation (1.5) can be calculated separately, then there is no cross terms. The folded potential $U(\mathbf{R})$ is the back Fourier transformation of the total potential $\tilde{U}(\mathbf{k})$.

$$U(\mathbf{R}) = (2\pi)^{-3} \int \tilde{U}(\mathbf{k}) e^{(-i\mathbf{k}\cdot\mathbf{R})} d\mathbf{k}.$$

$$U(R) = 8 \int k^2 j_0(kR) \tilde{v}(k) \left[\int j_0(kr_1) \rho_1(r_1) r_1^2 dr_1 \right] \left[\int j_0(kr_2) \rho_2(r_2) r_2^2 dr_2 \right] dk \quad (1.6)$$

This integral is easy to compute numerically, because it consists of three integrals each in one dimension.

1.3 Details of calculation

For all interactions the units of MeV and fm are used for the strengths of the interactions and the lengths respectively. In this work the nuclear interaction used is the well-known M3Y-Reid force [5, 37] in the form

$$v_n(r) = \frac{7999 e^{-4r}}{4r} - \frac{2134 e^{-2.5r}}{2.5r} - 262\delta(r) \quad MeV \quad (1.7)$$

making use of the Fourier transform; see (appendix 1-B.2)

$$\tilde{v}_n(k) = \frac{7999 \times 4\pi}{4[k^2 + 4^2]} - \frac{2134 \times 4\pi}{2.5[k^2 + 2.5^2]} - 262 \quad MeV fm^3 \quad (1.8)$$

Coulomb interaction between two charged nucleons (protons) in the two nuclei separated by distance (r) is given by

$$v_c(r) = (1.44) \left(\frac{1}{r} \right) \quad MeV \quad (1.9)$$

and its Fourier transform; see (appendix 1-B.1)

$$\tilde{v}_c(k) = \frac{4\pi \times 1.44}{k^2} \quad MeV fm^3 \quad (1.10)$$

The charge and matter density distribution can be described in the form of 2pF or 3pF distributions, given respectively by

$$\rho(r) = \frac{\rho_o}{1 + e^{\frac{r-R_o}{a}}} \quad (1.11 - A)$$

$$\rho(r) = \frac{\rho_o \left[1 + w \left(\frac{r}{R_0} \right)^2 \right]}{1 + e^{\frac{r-R_o}{a}}} \quad (1.11 - B)$$

where a is a parameter that measures the “diffuseness” of the nuclear surface, with typical values around 0.5 fm , and R_0 is the nuclear radius. The 2pF is the same as 3pF with ($w = 0$). Density distributions parameters are used as obtained from elastic electron scattering experiments [36] and are presented in table (1.1).

The net potential between two interacting nuclei is a sum of two parts, repulsive part plus attractive part.

$$U_{Net}(R) = U_{Coulomb}(R) + U_{Nuclear}(R)$$

each part in the above equation is a nucleus-nucleus interaction calculated in the frame work of the double folding model given by equation (1.6), then added to obtain the total interaction potential between the interacting pair. The radial distribution of the potential depends on the composition, shape, and orientation of the two interacting nuclei [53]. Similarly, the potential barrier parameters (R_B and V_B) depend on the same variables. The aim of this work is to study the dependence of Coulomb barrier parameters on the compositions of the target nucleus and the projectile nucleus, assuming that both nuclei have spherical shape and have ground state density described by 2pF or 3pF distributions. On the basis of the presented treatment, behavior of potential barrier parameters will be

discussed to show their systematic behavior with the composition of the interacting pair.

1.4 Numerical calculations and results

Table (1.1) density-distribution parameters obtained from elastic electron scattering [36]

<i>Nucleus</i>	R_0 <i>fm</i>	a <i>fm</i>	w
¹⁶ O	2.608	0.513	-0.051
¹⁹ F	2.59	0.564	
²⁰ Ne	2.74	0.569	
²² Ne	2.782	0.549	
²⁴ Mg	3.192	0.604	-0.249
²⁵ Mg	2.76	0.608	
²⁶ Mg	3.05	0.524	
²⁷ Al	2.84	0.569	
²⁸ Si	3.30	0.545	-0.18
²⁹ Si	3.17	0.52	
³¹ P	3.353	0.5789	-0.160
³² S	3.458	0.6098	-0.208
⁴⁰ Ar	3.73	0.62	-0.19
³⁹ K	3.743	0.585	-0.201
⁴⁰ Ca	3.766	0.586	-0.161
<i>Ti</i>	3.75	0.567	
⁵¹ V	3.91	0.532	
<i>Cr</i>	3.975	0.53	
⁵⁵ Mn	3.89	0.567	
<i>Fe</i>	3.98	0.569	
⁵⁴ Fe	4.012	0.5339	
⁵⁶ Fe	3.971	0.5935	
⁵⁸ Fe	4.027	0.5757	
⁵⁹ Co	4.08	0.569	
<i>Ni</i>	4.09	0.569	
⁵⁸ Ni	4.3092	0.5169	
⁶⁰ Ni	4.4891	0.5369	
⁶¹ Ni	4.4024	0.5401	
⁶² Ni	4.4425	0.5386	
⁶⁴ Ni	4.5211	0.5278	
<i>Cu</i>	4.2	0.569	
⁶³ Cu	4.214	0.586	
⁶⁵ Cu	4.271	0.579	
<i>Zn</i>	4.28	0.569	
⁶⁴ Zn	4.285	0.584	
⁶⁶ Zn	4.286	0.595	

<i>Nucleus</i>	R_0 <i>fm</i>	a <i>fm</i>	w
⁶⁸ Zn	4.353	0.567	
⁷⁰ Zn	4.409	0.583	
⁸⁸ Sr	4.83	0.496	
⁸⁹ Y	4.86	0.542	
⁹³ Nb	4.87	0.573	
¹¹⁰ Cd	5.33	0.535	
¹¹² Cd	5.38	0.532	
¹¹⁴ Cd	5.40	0.537	
¹¹⁶ Cd	5.42	0.532	
<i>In</i>	5.24	0.52	
¹¹² Sn	5.375	0.56	
¹¹⁶ Sn	5.416	0.552	
¹¹⁸ Sn	5.442	0.543	
¹²⁰ Sn	5.32	0.576	
¹²⁴ Sn	5.490	0.534	
<i>Sb</i>	5.32	0.57	
<i>La</i>	5.71	0.535	
¹⁴² Nd	5.6135	0.5868	0.096
¹⁴⁴ Nd	5.6256	0.6178	
¹⁴⁶ Nd	5.867	0.556	
¹⁴⁸ Nd	5.6703	0.644	
¹⁵⁰ Nd	5.865	0.571	
¹⁴⁸ Sm	5.771	0.596	
¹⁵⁴ Sm	5.9387	0.522	
¹⁶⁵ Ho	6.12	0.57	
¹⁸¹ Ta	6.38	0.64	
¹⁸⁴ W	6.51	0.535	
¹⁸⁶ W	6.58	0.480	
¹⁹⁷ Au	6.38	0.535	
<i>P[<i>l</i>b]</i>	6.69	0.494	
²⁰⁶ Pb	6.61	0.545	
²⁰⁷ Pb	6.62	0.546	
²⁰⁸ Pb	6.624	0.549	
²⁰⁹ Bi	6.75	0.468	
²³² Th	6.7915	0.571	
²³⁸ U	6.854	0.605	

In table (1.1), the parameters are tabulated for 2pF and 3pF distributions. The parameters tabulated without mass number are the results for targets of natural isotopic composition.

For trans-uranium elements ($Z \geq 93$) the density distribution parameters are approximated as following:

- 1) The radius parameter (R_0) [6]

$$R_0 = 1.28A^{1/3} - 0.76 + 0.8 A^{-1/3} \quad fm$$

- 2) The diffuseness parameter is selected to be (0.54 fm) for all trans-uranium elements

Density distribution for 4He projectile [5] is taken as

$$\text{Matter density} = 0.4229 e^{-0.7024 r^2} \quad fm^{-3}$$

$$\text{Charge density} = 0.5 \times \text{Matter density} \quad fm^{-3}$$

It is given in tables (1.2- a, b, c, d) the results for the barrier radius (R_B) and the barrier height (V_B) calculated by using DFM, and the values of Coulomb and nuclear interactions at separation R_B , denoted respectively by V_C and V_N , followed by graphs and fits showing the systematic behavior of the fusion barrier parameters.

Table (1.2-*a*) Barrier position (R_B), barrier height (V_B), Coulomb interaction at $R=R_B$ (V_C), and nuclear interaction at $R=R_B$ (V_N), for the reactions between different targets and ${}^4\text{He}$ as projectile.

Z_T	A_T	R_B <i>fm</i>	V_B <i>MeV</i>	V_C <i>MeV</i>	V_N <i>MeV</i>	Z_T	A_T	R_B <i>fm</i>	V_B <i>MeV</i>	V_C <i>MeV</i>	V_N <i>MeV</i>
8	16	7.313	2.907	3.149	-0.242	50	118	9.638	13.966	14.930	-0.963
9	19	7.638	3.122	3.392	-0.270	50	120	9.663	13.898	14.891	-0.993
10	20	7.688	3.439	3.745	-0.306	50	124	9.688	13.915	14.852	-0.937
10	22	7.713	3.442	3.733	-0.291	51	121	9.638	14.223	15.229	-1.007
12	24	7.563	4.302	4.564	-0.262	57	139	9.863	15.605	16.630	-1.025
12	25	7.888	4.010	4.379	-0.369	60	142	9.988	16.146	17.290	-1.144
12	26	7.763	4.113	4.450	-0.337	60	144	10.038	16.030	17.200	-1.169
13	27	7.788	4.424	4.805	-0.381	60	146	10.038	16.110	17.204	-1.094
14	28	7.688	4.874	5.240	-0.366	60	148	10.188	15.781	16.946	-1.164
14	29	7.788	4.782	5.175	-0.393	60	150	10.113	15.993	17.076	-1.083
15	31	7.888	5.086	5.472	-0.386	62	148	10.063	16.539	17.734	-1.195
16	32	7.913	5.420	5.815	-0.395	62	154	10.013	16.738	17.821	-1.083
18	40	8.288	5.825	6.249	-0.425	67	165	10.288	17.544	18.742	-1.198
19	39	8.113	6.271	6.740	-0.469	73	181	10.738	18.282	19.563	-1.281
20	40	8.188	6.524	7.031	-0.507	74	184	10.513	19.036	20.255	-1.219
22	48	8.388	6.978	7.550	-0.573	74	186	10.438	19.263	20.401	-1.139
23	51	8.388	7.322	7.892	-0.570	79	197	10.413	20.519	21.833	-1.313
24	52	8.413	7.622	8.211	-0.589	82	206	10.638	20.852	22.180	-1.327
25	55	8.513	7.838	8.453	-0.614	82	207	10.663	20.824	22.128	-1.304
26	54	8.438	8.243	8.869	-0.625	82	208	10.663	20.790	22.128	-1.337
26	56	8.638	8.009	8.663	-0.654	83	209	10.538	21.398	22.664	-1.265
26	58	8.638	8.024	8.664	-0.640	90	232	10.888	22.356	23.787	-1.431
27	59	8.638	8.339	8.997	-0.658	92	238	11.038	22.487	23.982	-1.495
28	58	8.463	8.867	9.523	-0.656	93	239	11.238	22.467	23.811	-1.343
28	60	8.538	8.841	9.437	-0.596	94	239	11.238	22.723	24.067	-1.343
28	61	8.563	8.778	9.411	-0.633	95	243	11.263	22.885	24.268	-1.384
28	62	8.588	8.757	9.383	-0.626	96	245	11.288	23.098	24.475	-1.377
28	64	8.638	8.736	9.329	-0.593	97	247	11.313	23.305	24.674	-1.369
29	63	8.788	8.797	9.498	-0.701	98	249	11.313	23.512	24.928	-1.416
29	65	8.838	8.766	9.444	-0.678	99	254	11.363	23.650	25.073	-1.423
30	64	8.813	9.073	9.797	-0.724	100	253	11.363	23.925	25.324	-1.400
30	66	8.888	9.003	9.715	-0.711	101	255	11.363	24.130	25.577	-1.447
30	68	8.863	9.055	9.742	-0.687	102	255	11.363	24.384	25.830	-1.447
30	70	8.988	8.928	9.606	-0.677	103	257	11.388	24.589	26.027	-1.438
38	88	8.988	11.375	12.169	-0.795	104	261	11.413	24.746	26.222	-1.476
39	89	9.163	11.435	12.251	-0.815	105	262	11.413	24.974	26.474	-1.500
41	93	9.263	11.859	12.739	-0.880	106	263	11.438	25.204	26.669	-1.466
48	110	9.513	13.596	14.522	-0.926	107	262	11.413	25.478	26.978	-1.500
48	112	9.538	13.542	14.484	-0.942	108	265	11.438	25.658	27.172	-1.514
48	114	9.588	13.477	14.407	-0.930	109	266	11.438	25.883	27.421	-1.538
48	116	9.613	13.466	14.370	-0.904	110	269	11.463	26.062	27.614	-1.552
49	115	9.388	14.038	15.022	-0.984	111	272	11.488	26.238	27.803	-1.565
50	112	9.588	13.997	15.008	-1.011	112	277	11.538	26.366	27.931	-1.565
50	116	9.638	13.962	14.929	-0.968	114	289	11.663	26.578	28.126	-1.548

Table (1.2-*b*) The same as Table (1.2-*a*) but for ^{16}O projectile.

Z_T	A_T	R_B <i>fm</i>	V_B <i>MeV</i>	V_C <i>MeV</i>	V_N <i>MeV</i>	Z_T	A_T	R_B <i>fm</i>	V_B <i>MeV</i>	V_C <i>MeV</i>	V_N <i>MeV</i>
8	16	8.488	10.006	10.849	-0.842	50	118	10.638	50.309	54.089	-3.781
9	19	8.738	10.902	11.855	-0.953	50	120	10.663	50.194	53.963	-3.769
10	20	8.788	12.044	13.099	-1.055	50	124	10.713	50.083	53.710	-3.627
10	22	8.838	12.012	13.025	-1.013	51	121	10.638	51.333	55.175	-3.843
12	24	8.713	14.748	15.838	-1.090	57	139	10.863	56.309	60.380	-4.071
12	25	8.963	14.154	15.412	-1.258	60	142	10.938	58.649	63.137	-4.489
12	26	8.888	14.338	15.541	-1.203	60	144	10.988	58.347	62.832	-4.485
13	27	8.863	15.515	16.884	-1.370	60	146	11.038	58.362	62.565	-4.203
14	28	8.813	16.891	18.279	-1.388	60	148	11.113	57.625	62.124	-4.499
14	29	8.913	16.688	18.080	-1.392	60	150	11.088	58.024	62.280	-4.255
15	31	8.988	17.756	19.204	-1.449	62	148	11.038	60.135	64.652	-4.517
16	32	9.013	18.913	20.415	-1.502	62	154	11.013	60.443	64.792	-4.349
18	40	9.363	20.514	22.120	-1.607	67	165	11.263	63.803	68.458	-4.655
19	39	9.213	21.997	23.732	-1.736	73	181	11.638	67.110	72.179	-5.069
20	40	9.263	22.986	24.851	-1.865	74	184	11.513	69.223	73.962	-4.739
22	48	9.463	24.738	26.762	-2.023	74	186	11.438	69.702	74.449	-4.748
23	51	9.463	25.865	27.975	-2.110	79	197	11.388	74.525	79.830	-5.306
24	52	9.488	26.942	29.115	-2.173	82	206	11.613	75.969	81.245	-5.276
25	55	9.538	27.837	30.168	-2.331	82	207	11.638	75.877	81.072	-5.195
26	54	9.488	29.175	31.539	-2.363	82	208	11.638	75.778	81.071	-5.292
26	56	9.663	28.588	30.968	-2.380	83	209	11.563	77.469	82.594	-5.125
26	58	9.688	28.578	30.890	-2.312	90	232	11.838	81.773	87.486	-5.713
27	59	9.663	29.693	32.161	-2.468	92	238	11.963	82.560	88.486	-5.926
28	58	9.538	31.299	33.789	-2.490	93	239	12.188	82.300	87.794	-5.493
28	60	9.613	31.150	33.516	-2.366	94	239	12.188	83.244	88.738	-5.493
28	61	9.638	31.013	33.435	-2.422	95	243	12.213	83.862	89.496	-5.634
28	62	9.663	30.933	33.347	-2.414	96	245	12.238	84.659	90.272	-5.613
28	64	9.713	30.825	33.175	-2.350	97	247	12.238	85.435	91.211	-5.776
29	63	9.813	31.450	34.012	-2.562	98	249	12.263	86.210	91.962	-5.751
29	65	9.863	31.327	33.840	-2.513	99	254	12.313	86.746	92.526	-5.780
30	64	9.838	32.454	35.094	-2.640	100	253	12.288	87.756	93.645	-5.889
30	66	9.888	32.254	34.919	-2.664	101	255	12.313	88.527	94.388	-5.861
30	68	9.888	32.330	34.917	-2.587	102	255	12.313	89.461	95.323	-5.861
30	70	9.988	31.970	34.567	-2.597	103	257	12.313	90.232	96.258	-6.026
38	88	10.063	40.442	43.464	-3.021	104	261	12.363	90.834	96.800	-5.966
39	89	10.188	40.929	44.060	-3.131	105	262	12.363	91.682	97.729	-6.047
41	93	10.263	42.625	45.978	-3.354	106	263	12.363	92.537	98.668	-6.131
48	110	10.513	48.877	52.546	-3.669	107	262	12.338	93.545	99.792	-6.247
48	112	10.563	48.686	52.298	-3.612	108	265	12.363	94.228	100.527	-6.299
48	114	10.613	48.489	52.049	-3.560	109	266	12.363	95.065	101.448	-6.383
48	116	10.613	48.426	52.048	-3.623	110	269	12.388	95.745	102.178	-6.433
49	115	10.438	50.315	54.027	-3.712	111	272	12.413	96.413	102.895	-6.481
50	112	10.588	50.500	54.344	-3.845	112	277	12.463	96.914	103.401	-6.488
50	116	10.638	50.337	54.088	-3.751	114	289	12.588	97.764	104.206	-6.441

Table (1.2-c) The same as Table (1.2-a) but for ^{40}Ca projectile.

Z_T	A_T	R_B <i>fm</i>	V_B <i>MeV</i>	V_C <i>MeV</i>	V_N <i>MeV</i>	Z_T	A_T	R_B <i>fm</i>	V_B <i>MeV</i>	V_C <i>MeV</i>	V_N <i>MeV</i>
8	16	9.263	22.986	24.851	-1.865	50	118	11.338	117.998	126.866	-8.868
9	19	9.488	25.170	27.294	-2.124	50	120	11.338	117.827	126.867	-9.040
10	20	9.513	27.838	30.251	-2.414	50	124	11.413	117.454	126.031	-8.577
10	22	9.588	27.740	30.015	-2.274	51	121	11.313	120.468	129.699	-9.231
12	24	9.488	33.857	36.358	-2.501	57	139	11.563	132.216	141.802	-9.585
12	25	9.688	32.811	35.645	-2.834	60	142	11.613	138.037	148.659	-10.621
12	26	9.638	33.108	35.827	-2.719	60	144	11.663	137.440	147.980	-10.540
13	27	9.613	35.884	38.916	-3.032	60	146	11.713	137.272	147.388	-10.116
14	28	9.588	38.929	42.001	-3.072	60	148	11.788	135.927	146.407	-10.480
14	29	9.663	38.552	41.690	-3.138	60	150	11.763	136.561	146.755	-10.195
15	31	9.738	41.030	44.310	-3.280	62	148	11.713	141.616	152.304	-10.689
16	32	9.763	43.696	47.111	-3.416	62	154	11.713	142.020	152.290	-10.270
18	40	10.088	47.584	51.322	-3.738	67	165	11.938	150.345	161.457	-11.111
19	39	9.938	50.941	54.998	-4.057	73	181	12.288	158.785	170.893	-12.108
20	40	9.988	53.316	57.614	-4.298	74	184	12.188	163.207	174.655	-11.448
22	48	10.188	57.526	62.138	-4.613	74	186	12.138	164.059	175.379	-11.320
23	51	10.213	60.087	64.798	-4.711	79	197	12.088	175.593	188.008	-12.415
24	52	10.213	62.604	67.616	-5.012	82	206	12.288	179.263	191.944	-12.681
25	55	10.263	64.787	70.088	-5.300	82	207	12.313	179.060	191.556	-12.496
26	54	10.213	67.820	73.244	-5.424	82	208	12.313	178.850	191.554	-12.704
26	56	10.363	66.664	72.185	-5.521	83	209	12.263	182.423	194.685	-12.263
26	58	10.388	66.599	72.015	-5.416	90	232	12.513	193.304	206.904	-13.600
27	59	10.388	69.191	74.785	-5.594	92	238	12.638	195.470	209.387	-13.916
28	58	10.288	72.720	78.310	-5.590	93	239	12.863	194.792	207.953	-13.161
28	60	10.338	72.348	77.909	-5.561	94	239	12.838	197.030	210.597	-13.568
28	61	10.388	72.095	77.548	-5.453	95	243	12.888	198.526	212.006	-13.480
28	62	10.413	71.913	77.358	-5.446	96	245	12.888	200.433	214.284	-13.850
28	64	10.463	71.649	76.986	-5.337	97	247	12.913	202.292	216.092	-13.800
29	63	10.513	73.411	79.363	-5.952	98	249	12.938	204.145	217.893	-13.748
29	65	10.563	73.122	78.988	-5.866	99	254	12.988	205.459	219.279	-13.820
30	64	10.538	75.776	81.902	-6.126	100	253	12.963	207.847	221.906	-14.059
30	66	10.588	75.358	81.520	-6.163	101	255	12.963	209.691	224.121	-14.430
30	68	10.588	75.450	81.515	-6.065	102	255	12.963	211.911	226.341	-14.430
30	70	10.713	74.701	80.563	-5.862	103	257	12.988	213.755	228.123	-14.368
38	88	10.788	94.320	101.350	-7.030	104	261	13.013	215.220	229.896	-14.676
39	89	10.888	95.679	103.061	-7.382	105	262	13.013	217.240	232.104	-14.864
41	93	10.963	99.799	107.599	-7.800	106	263	13.013	219.277	234.333	-15.055
48	110	11.213	114.528	123.156	-8.628	107	262	12.988	221.662	236.980	-15.318
48	112	11.263	114.099	122.611	-8.513	108	265	13.013	223.309	238.748	-15.439
48	114	11.313	113.673	122.062	-8.389	109	266	13.013	225.304	240.937	-15.633
48	116	11.338	113.514	121.793	-8.280	110	269	13.063	226.945	242.230	-15.286
49	115	11.138	117.760	126.571	-8.811	111	272	13.088	228.559	243.954	-15.395
50	112	11.288	118.494	127.428	-8.934	112	277	13.138	229.791	245.207	-15.416
50	116	11.338	118.095	126.863	-8.768	114	289	13.263	231.912	247.241	-15.329

Table (1.2-d) The same as Table (1.2-a) but for ^{60}Ni projectile.

Z_T	A_T	R_B <i>fm</i>	V_B <i>MeV</i>	V_C <i>MeV</i>	V_N <i>MeV</i>	Z_T	A_T	R_B <i>fm</i>	V_B <i>MeV</i>	V_C <i>MeV</i>	V_N <i>MeV</i>
8	16	9.613	31.150	33.516	-2.366	50	118	11.713	160.648	171.882	-11.234
9	19	9.838	34.132	36.842	-2.710	50	120	11.713	160.430	171.884	-11.453
10	20	9.888	37.746	40.736	-2.990	50	124	11.763	159.941	171.149	-11.207
10	22	9.938	37.631	40.531	-2.900	51	121	11.688	164.012	175.707	-11.696
12	24	9.838	45.875	49.077	-3.201	57	139	11.913	180.089	192.640	-12.552
12	25	10.038	44.512	48.151	-3.639	60	142	11.988	188.056	201.562	-13.506
12	26	10.013	44.914	48.267	-3.353	60	144	12.013	187.265	201.086	-13.821
13	27	9.963	48.671	52.555	-3.885	60	146	12.088	187.037	199.892	-12.855
14	28	9.938	52.779	56.717	-3.938	60	148	12.138	185.266	199.011	-13.745
14	29	10.013	52.291	56.312	-4.021	60	150	12.138	186.103	199.060	-12.956
15	31	10.088	55.653	59.867	-4.215	62	148	12.063	192.962	206.988	-14.026
16	32	10.113	59.256	63.657	-4.402	62	154	12.088	193.505	206.538	-13.033
18	40	10.438	64.600	69.425	-4.825	67	165	12.313	204.945	219.098	-14.153
19	39	10.313	69.120	74.179	-5.059	73	181	12.663	216.622	232.105	-15.483
20	40	10.338	72.348	77.909	-5.561	74	184	12.538	222.562	237.628	-15.067
22	48	10.538	78.124	84.083	-5.959	74	186	12.513	223.696	238.109	-14.413
23	51	10.563	81.607	87.689	-6.081	79	197	12.438	239.414	255.739	-16.325
24	52	10.588	85.021	91.286	-6.265	82	206	12.663	244.513	260.696	-16.184
25	55	10.638	88.005	94.641	-6.636	82	207	12.663	244.245	260.698	-16.453
26	54	10.563	92.093	99.120	-7.027	82	208	12.688	243.968	260.182	-16.215
26	56	10.738	90.570	97.507	-6.936	83	209	12.638	248.781	264.404	-15.623
26	58	10.763	90.493	97.284	-6.791	90	232	12.863	263.790	281.711	-17.921
27	59	10.763	94.008	101.026	-7.019	92	238	12.988	266.822	285.169	-18.347
28	58	10.638	98.749	105.999	-7.250	93	239	13.213	265.958	283.348	-17.390
28	60	10.713	98.258	105.229	-6.970	94	239	13.213	269.005	286.395	-17.390
28	61	10.738	97.932	105.002	-7.069	95	243	13.238	271.068	288.886	-17.818
28	62	10.763	97.693	104.753	-7.060	96	245	13.263	273.681	291.441	-17.760
28	64	10.813	97.352	104.265	-6.913	97	247	13.288	276.222	293.917	-17.694
29	63	10.863	99.768	107.502	-7.734	98	249	13.288	278.760	296.940	-18.180
29	65	10.913	99.392	107.010	-7.618	99	254	13.338	280.580	298.856	-18.277
30	64	10.888	102.982	110.950	-7.968	100	253	13.313	283.825	302.422	-18.598
30	66	10.963	102.435	110.197	-7.762	101	255	13.338	286.351	304.870	-18.519
30	68	10.963	102.566	110.191	-7.625	102	255	13.313	289.370	308.466	-19.097
30	70	11.063	101.578	109.192	-7.615	103	257	13.338	291.896	310.910	-19.014
38	88	11.163	128.258	137.088	-8.830	104	261	13.388	293.915	312.757	-18.842
39	89	11.263	130.137	139.445	-9.309	105	262	13.388	296.673	315.761	-19.088
41	93	11.313	135.766	145.942	-10.177	106	263	13.388	299.454	318.791	-19.338
48	110	11.588	155.872	166.795	-10.923	107	262	13.363	302.695	322.376	-19.681
48	112	11.638	155.307	166.081	-10.774	108	265	13.388	304.958	324.799	-19.841
48	114	11.663	154.748	165.715	-10.967	109	266	13.388	307.684	327.777	-20.094
48	116	11.688	154.543	165.361	-10.818	110	269	13.413	309.938	330.186	-20.248
49	115	11.513	160.253	171.382	-11.129	111	272	13.438	312.155	332.551	-20.396
50	112	11.638	161.289	172.989	-11.700	112	277	13.488	313.866	334.291	-20.425
50	116	11.688	160.771	172.245	-11.474	114	289	13.613	316.836	337.146	-20.310

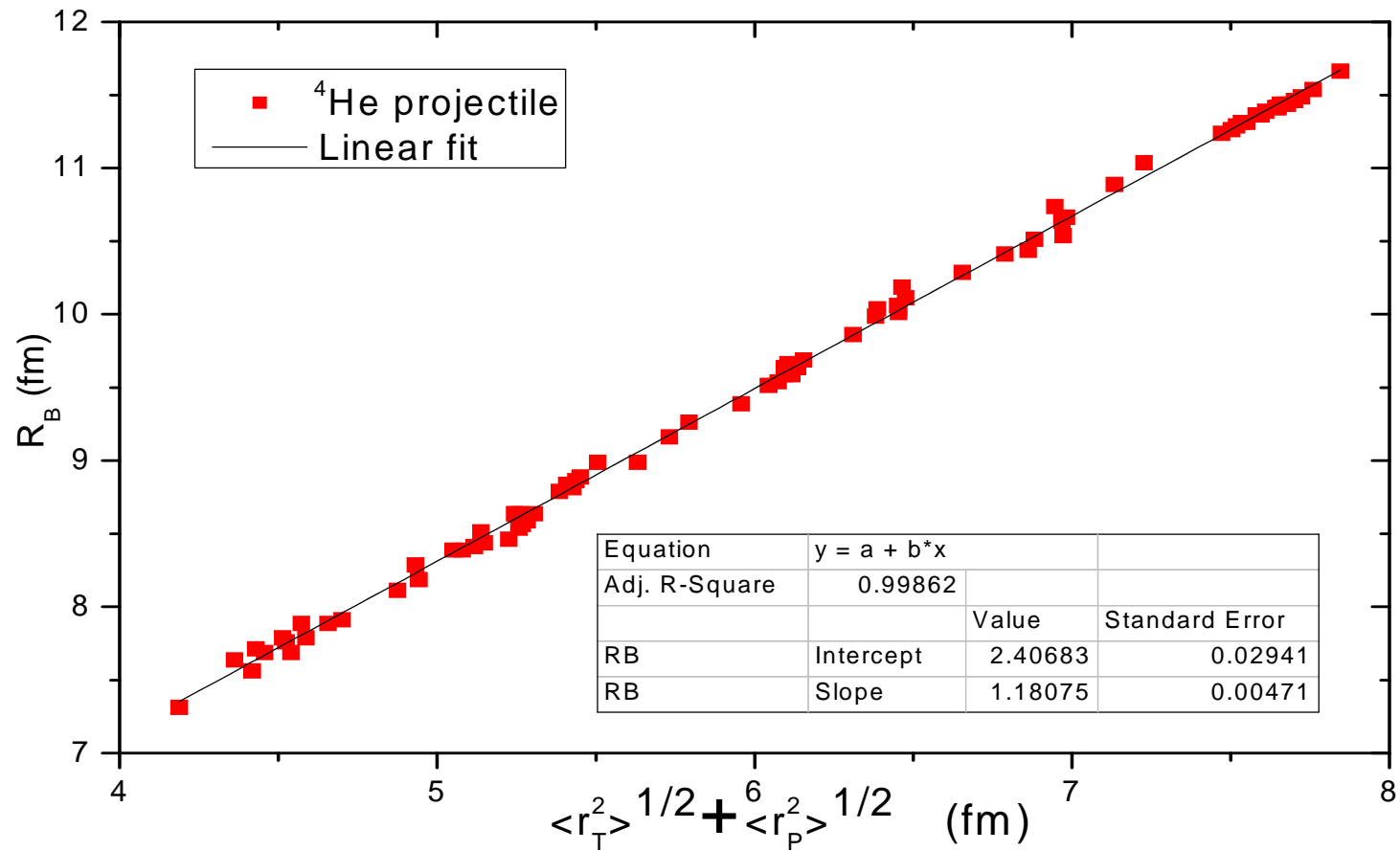


Figure (1.2-a) The variation of calculated barrier position (R_B) with $\langle r_T^2 \rangle^{1/2} + \langle r_P^2 \rangle^{1/2}$ for the reactions with ${}^4\text{He}$. The solid line is a linear fit to data and represented by

$$R_B = (1.18075 \pm 0.00471) \left(\langle r_T^2 \rangle^{1/2} + \langle r_P^2 \rangle^{1/2} \right) + (2.40683 \pm 0.02941)$$

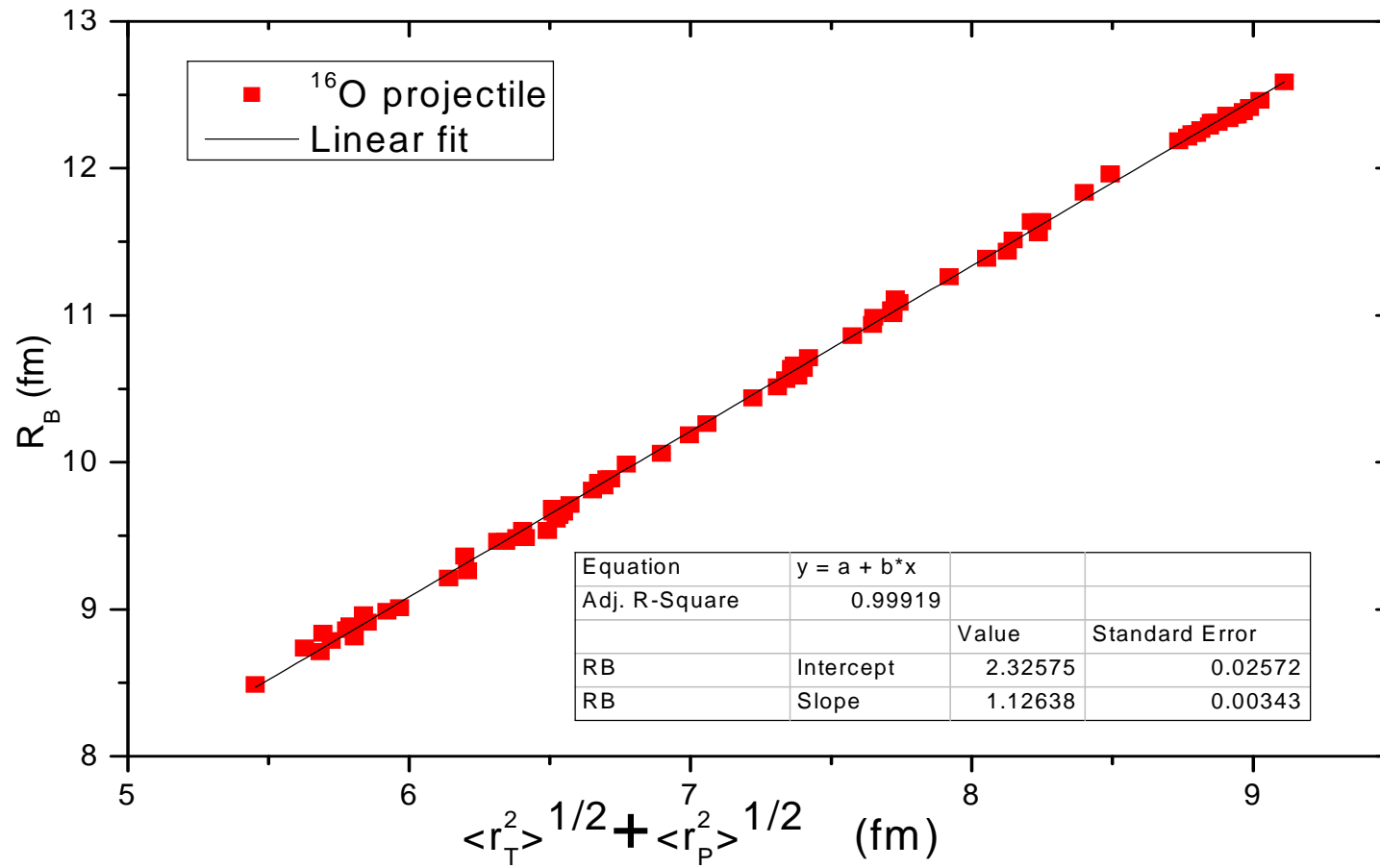


Figure (1.2-b) The same as Figure (1.2-a) but for ^{16}O as projectile. The solid line is a linear fit to data and represented by

$$R_B = (1.12638 \pm 0.00343) \left(\langle r_T^2 \rangle^{\frac{1}{2}} + \langle r_P^2 \rangle^{\frac{1}{2}} \right) + (2.32575 \pm 0.02572)$$

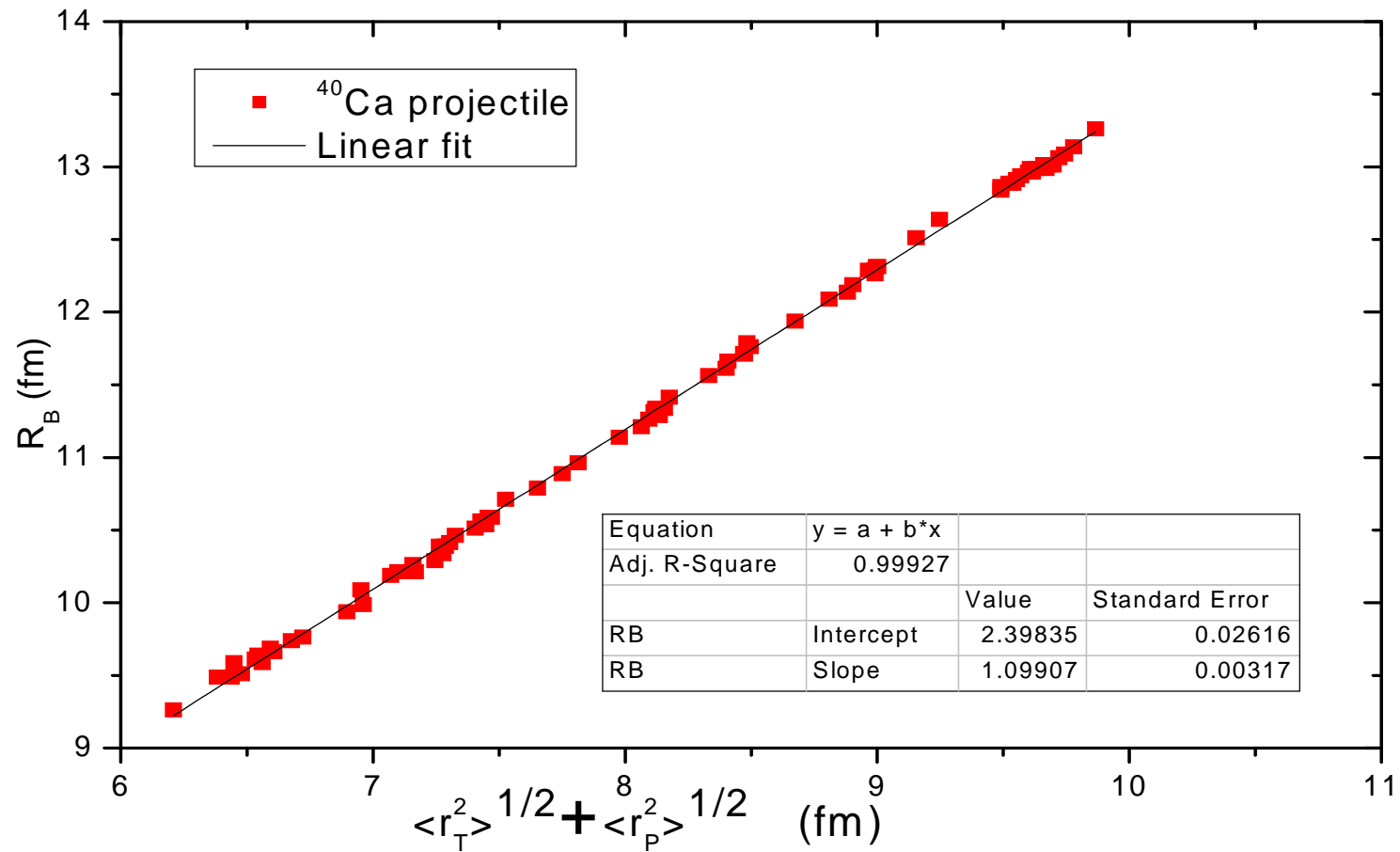


Figure (1.2-c) The same as Figure (1.2-a) but for ^{40}Ca as projectile. The solid line is a linear fit to data and represented by

$$R_B = (1.09907 \pm 0.00317) \left(\langle r_T^2 \rangle^{\frac{1}{2}} + \langle r_P^2 \rangle^{\frac{1}{2}} \right) + (2.39835 \pm 0.02616)$$

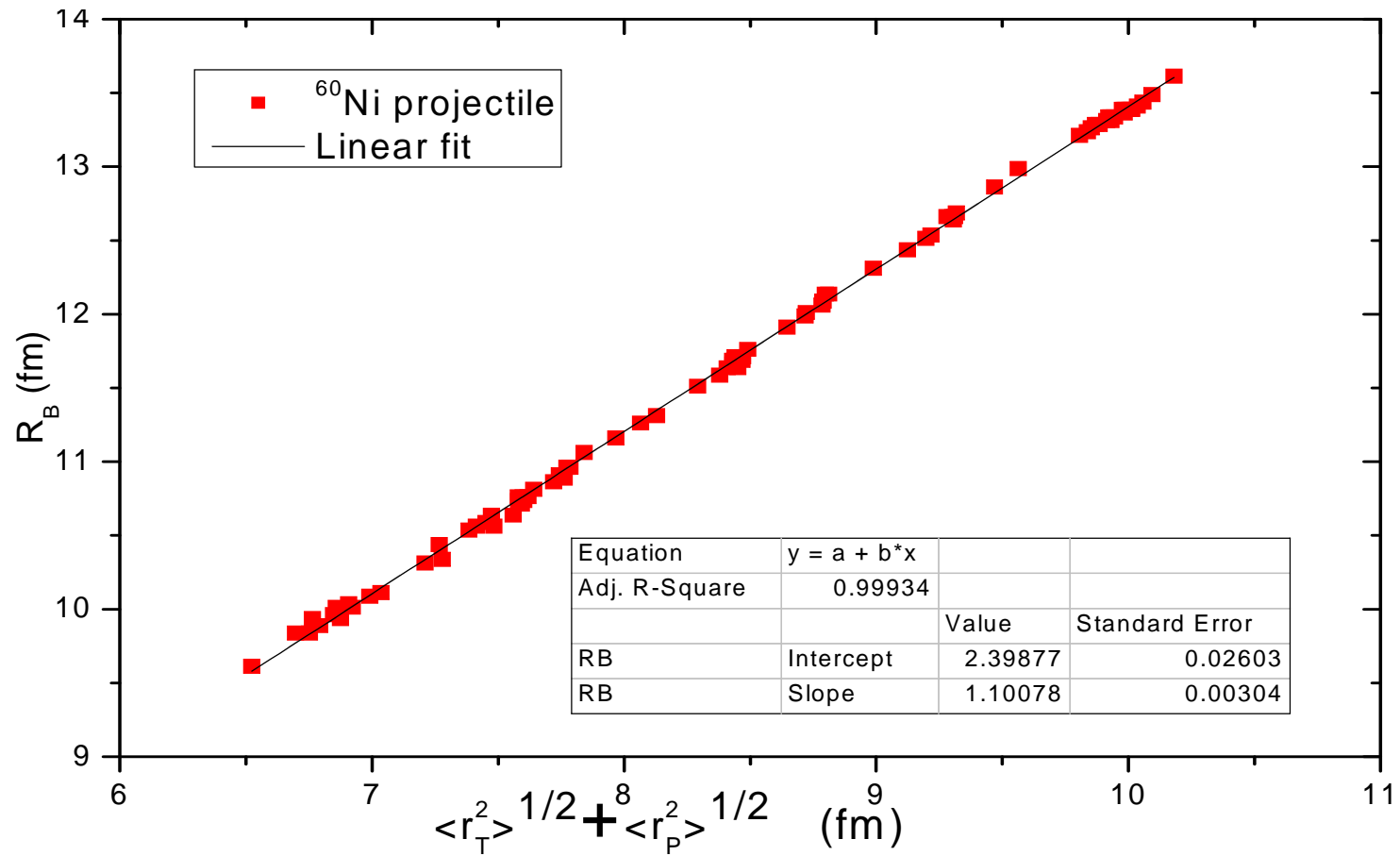


Figure (1.2-d) The same as Figure (1.2-a) but for ^{60}Ni as projectile. The solid line is a linear fit to data and represented by

$$R_B = (1.10078 \pm 0.00304) \left(\langle r_T^2 \rangle^{\frac{1}{2}} + \langle r_P^2 \rangle^{\frac{1}{2}} \right) + (2.39877 \pm 0.02603)$$

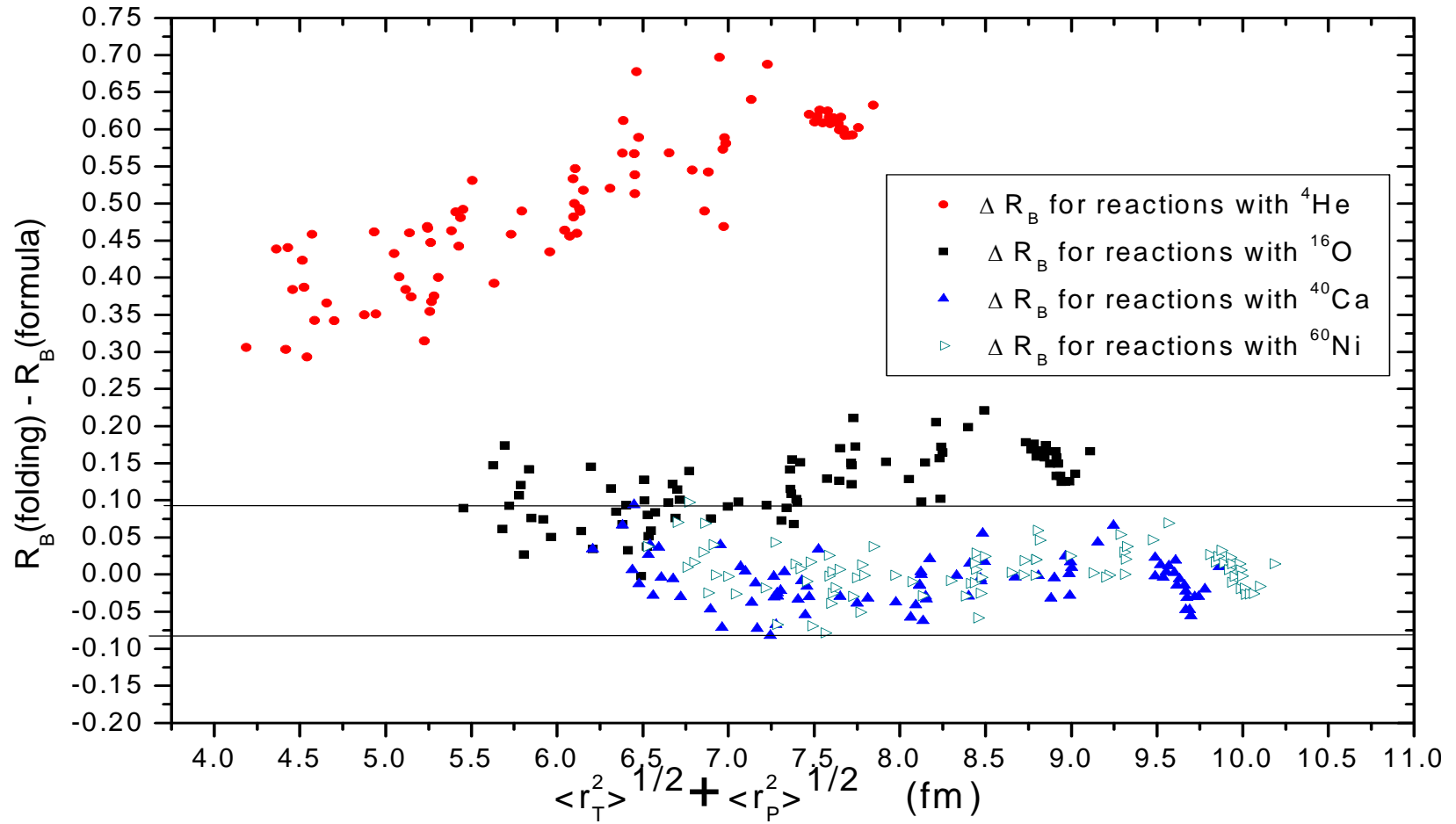


Figure (1.3-a) The differences between the values of R_B calculated using DFMA analysis and the values calculated using the formula $R_B = 1.1 \left(\langle r_T^2 \rangle^{\frac{1}{2}} + \langle r_P^2 \rangle^{\frac{1}{2}} \right) + 2.4$.

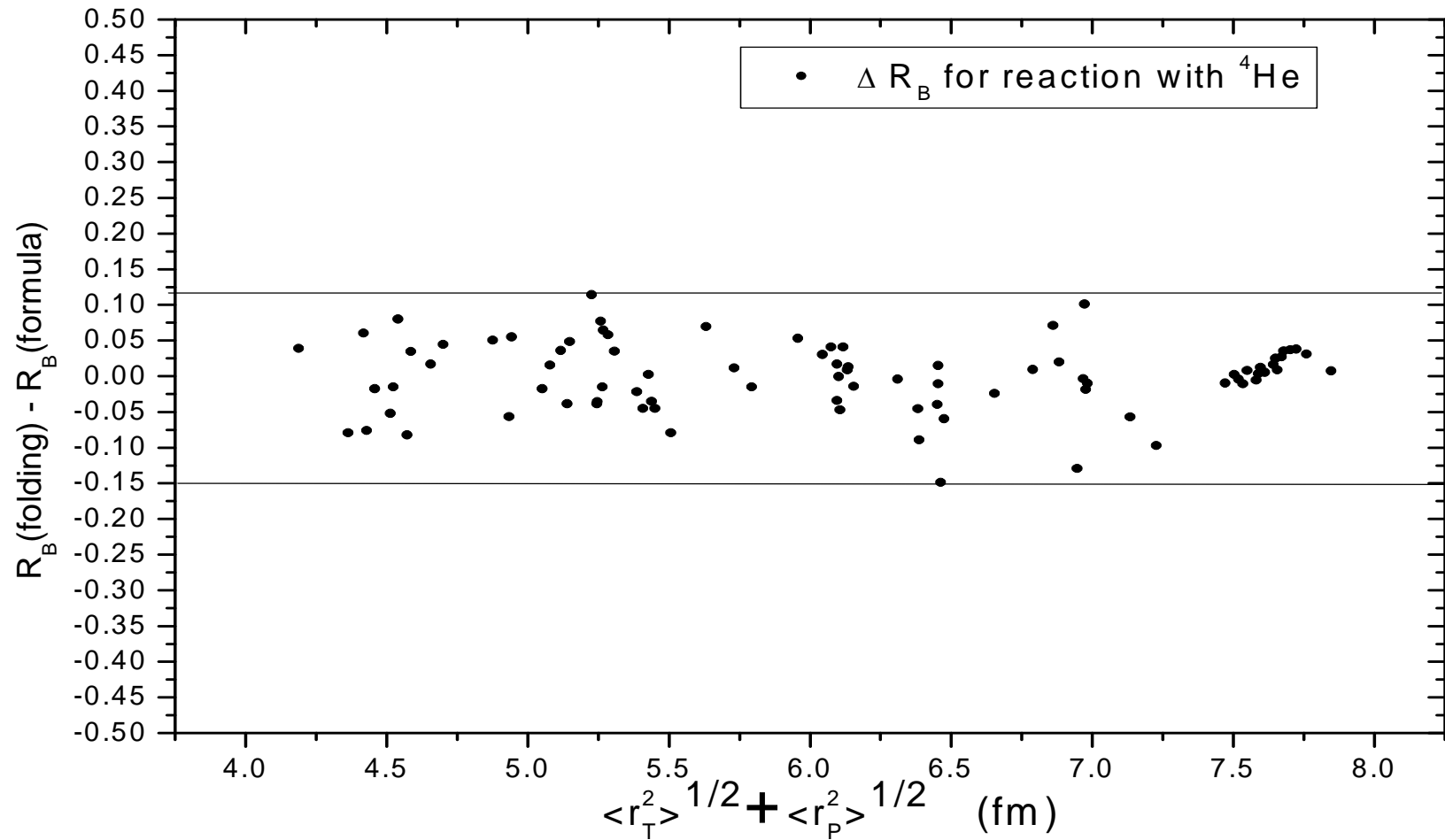


Figure (1.3-b) The differences between the values of R_B calculated using DFM analysis and the values calculated using the formula $\left[R_B = 1.18075 \left(\langle r_T^2 \rangle^{\frac{1}{2}} + \langle r_P^2 \rangle^{\frac{1}{2}} \right) + 2.40683 \right]$, for reactions with ${}^4\text{He}$.

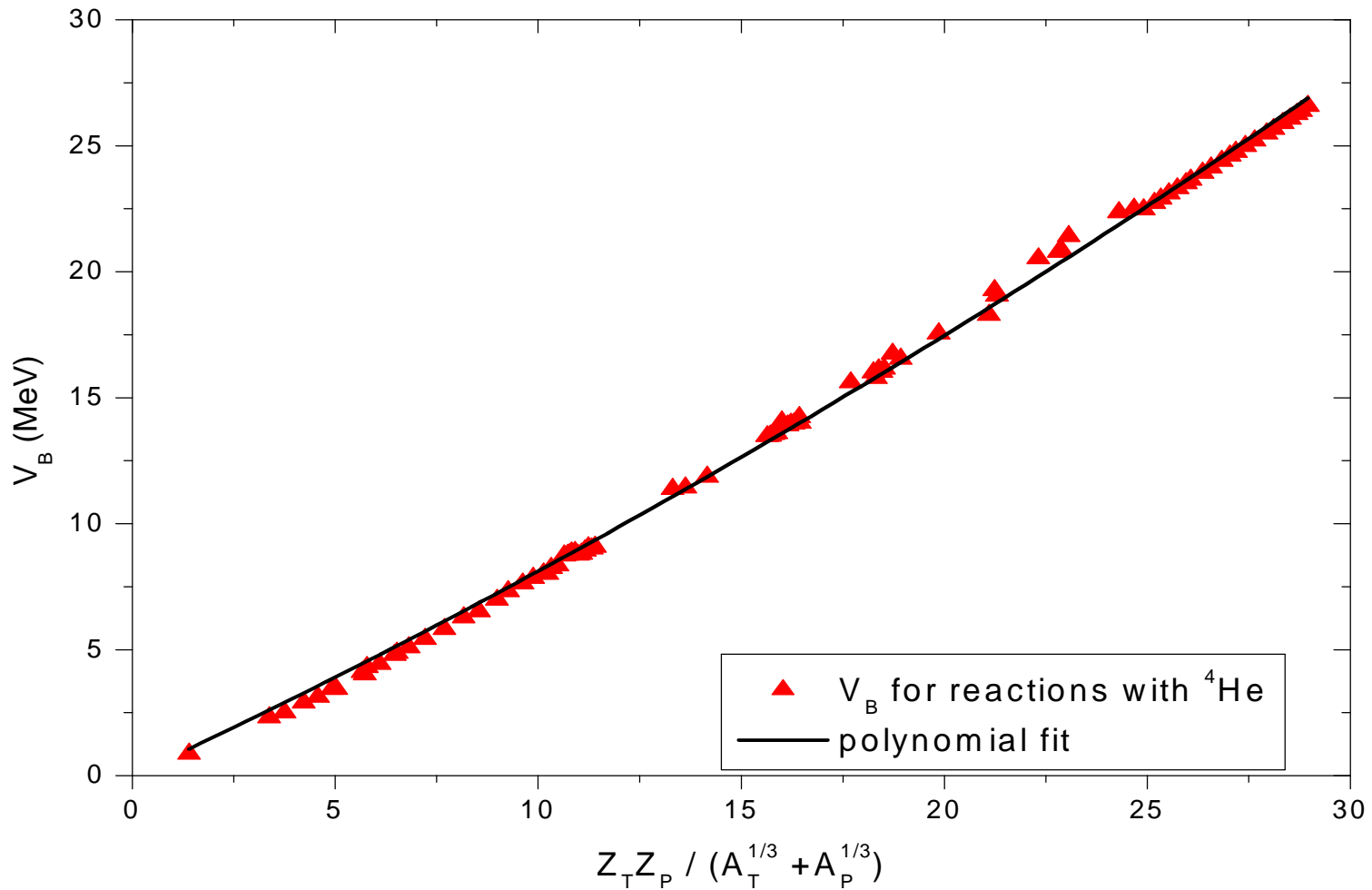


Figure (1.4-a) The variation of calculated barrier height (V_B) with $Z_1 Z_2 / (A_T^{1/3} + A_P^{1/3})$ for the reactions with ${}^4\text{He}$. The solid line is a second order polynomial fit to data and represented by

$$V_B = (0.74999 \pm 0.00681) \frac{Z_T Z_P}{A_T^{1/3} + A_P^{1/3}} + (6.15 \pm 0.292177) \times 10^{-3} \left[\frac{Z_T Z_P}{A_T^{1/3} + A_P^{1/3}} \right]^2$$

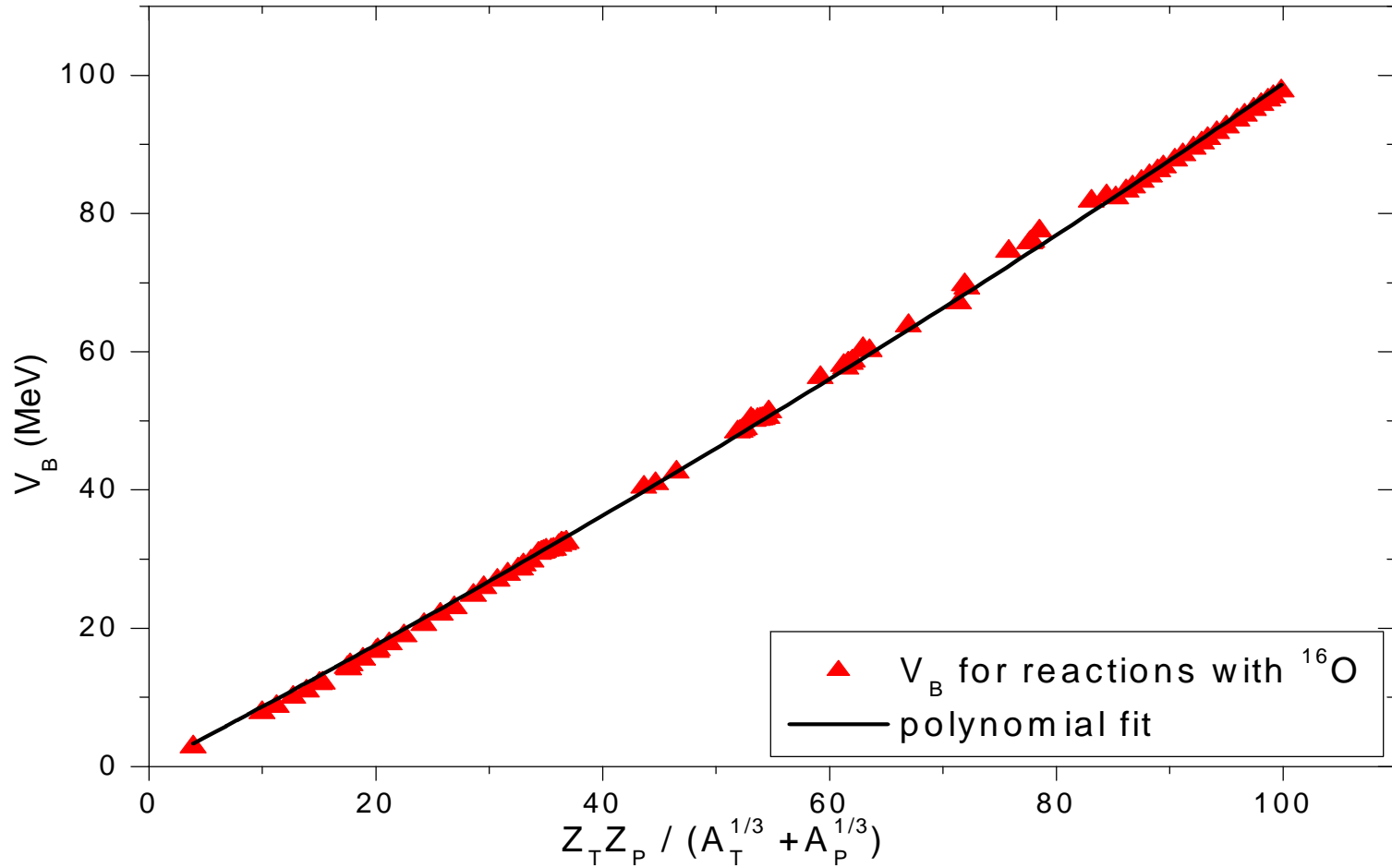


Figure (1.4-*b*) The same as Figure (1.4-*a*) but for ^{16}O as projectile. The solid line is a second order polynomial fit to data and represented by

$$V_B = (0.8529 \pm 0.00561) \frac{Z_T Z_P}{A_T^{1/3} + A_P^{1/3}} + (13.5 \pm 0.69832) \times 10^{-4} \left[\frac{Z_T Z_P}{A_T^{1/3} + A_P^{1/3}} \right]^2$$

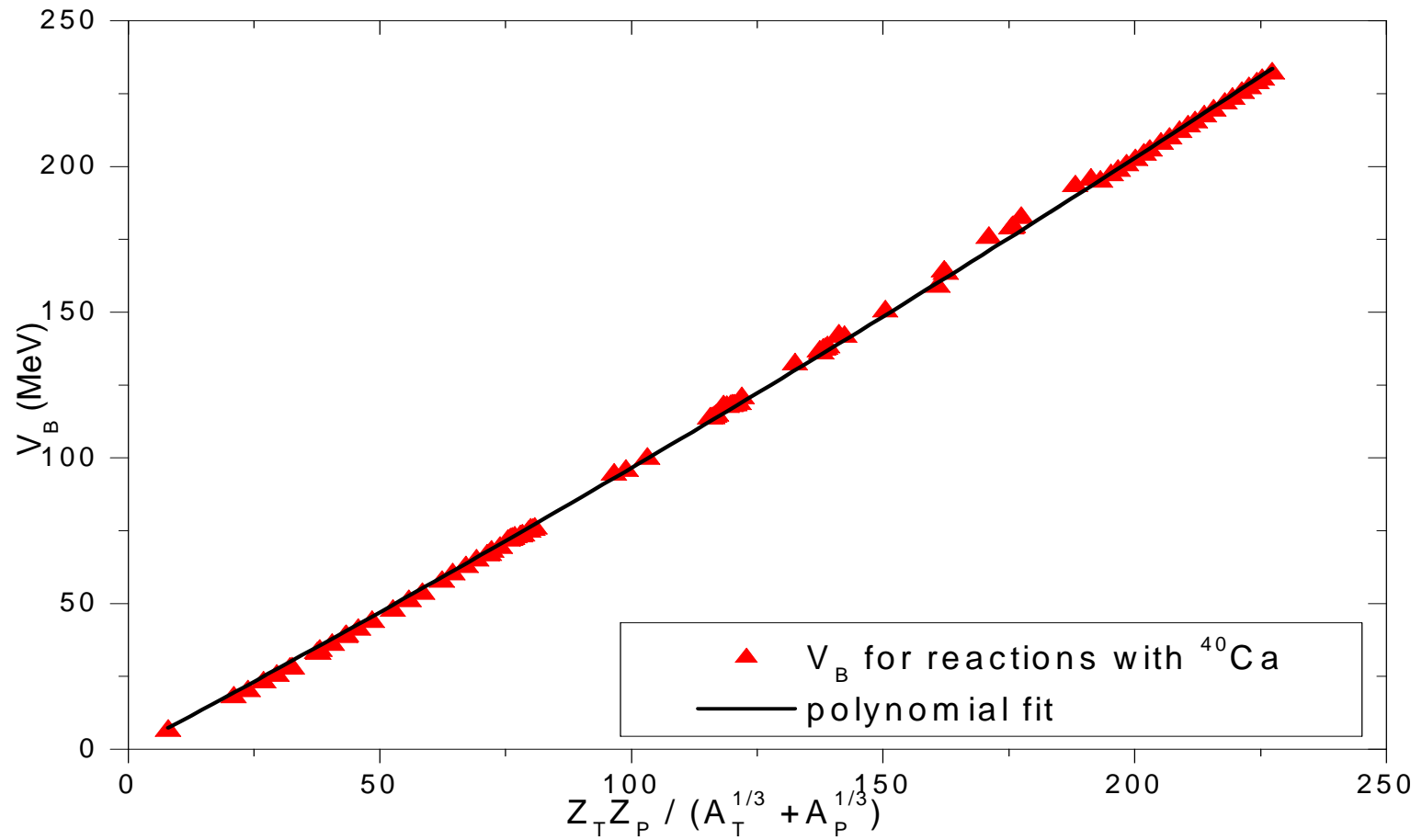


Figure (1.4-c) The same as Figure (1.4-a) but for ^{40}Ca as projectile. The solid line is a second order polynomial fit to data and represented by

$$V_B = (0.91656 \pm 0.00503) \frac{Z_T Z_P}{A_T^{1/3} + A_P^{1/3}} + (4.89575 \pm 0.275422) \times 10^{-4} \left[\frac{Z_T Z_P}{A_T^{1/3} + A_P^{1/3}} \right]^2$$

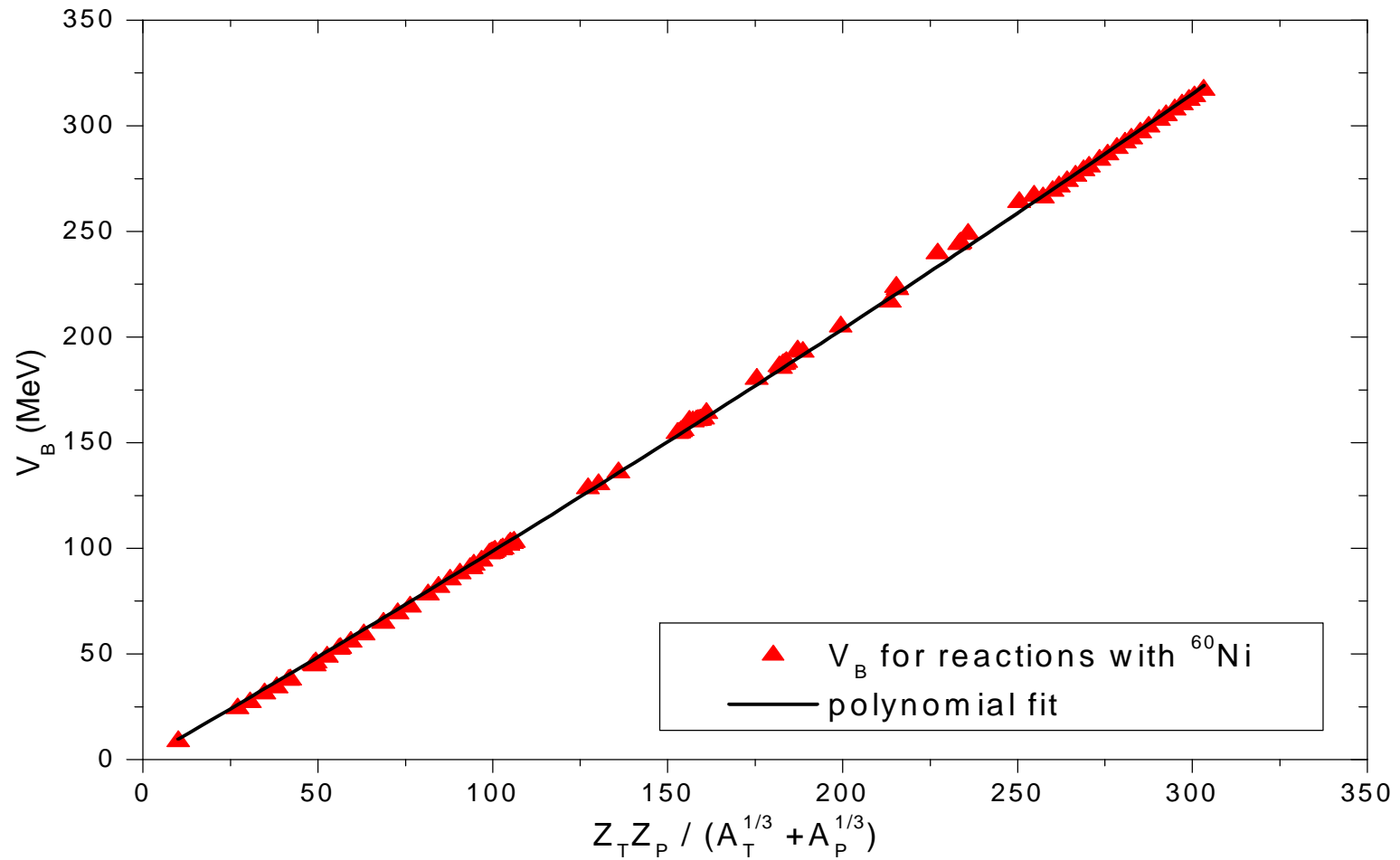


Figure (1.4-d) The same as Figure (1.4-a) but for ^{60}Ni as projectile. The solid line is a second order polynomial fit to data and represented by

$$V_B = (0.95546 \pm 0.00477) \frac{Z_T Z_P}{A_T^{1/3} + A_P^{1/3}} + (3.17332 \pm 0.195828) \times 10^{-4} \left[\frac{Z_T Z_P}{A_T^{1/3} + A_P^{1/3}} \right]^2$$

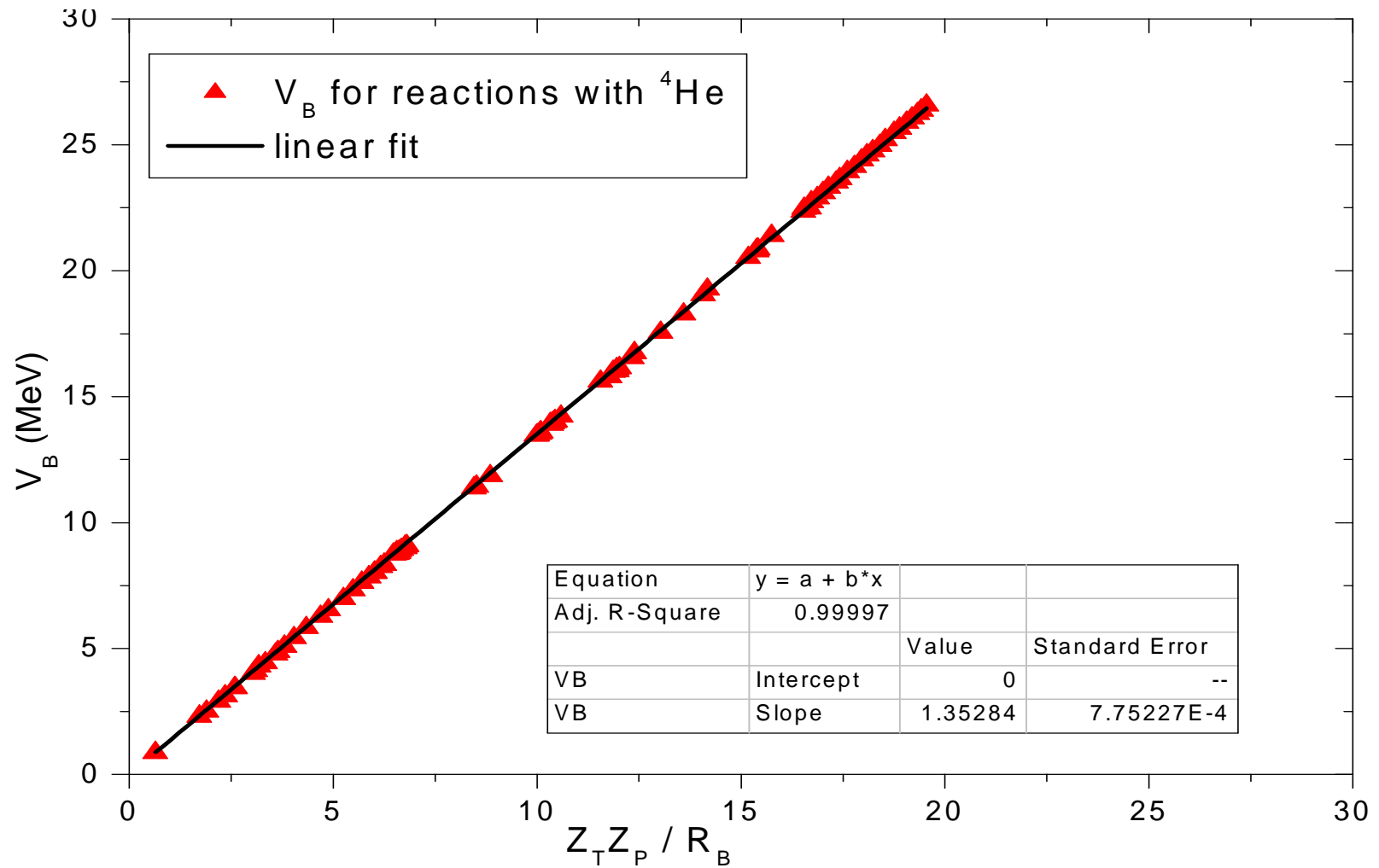


Figure (1.5-a) The variation of calculated barrier height (V_B) with $(Z_T Z_P / R_B)$ for the reactions with ${}^4\text{He}$. The solid line is a linear fit to data and represented by

$$V_B = (1.35284 \pm 7.75227 \times 10^{-4}) \times Z_T Z_P / R_B .$$

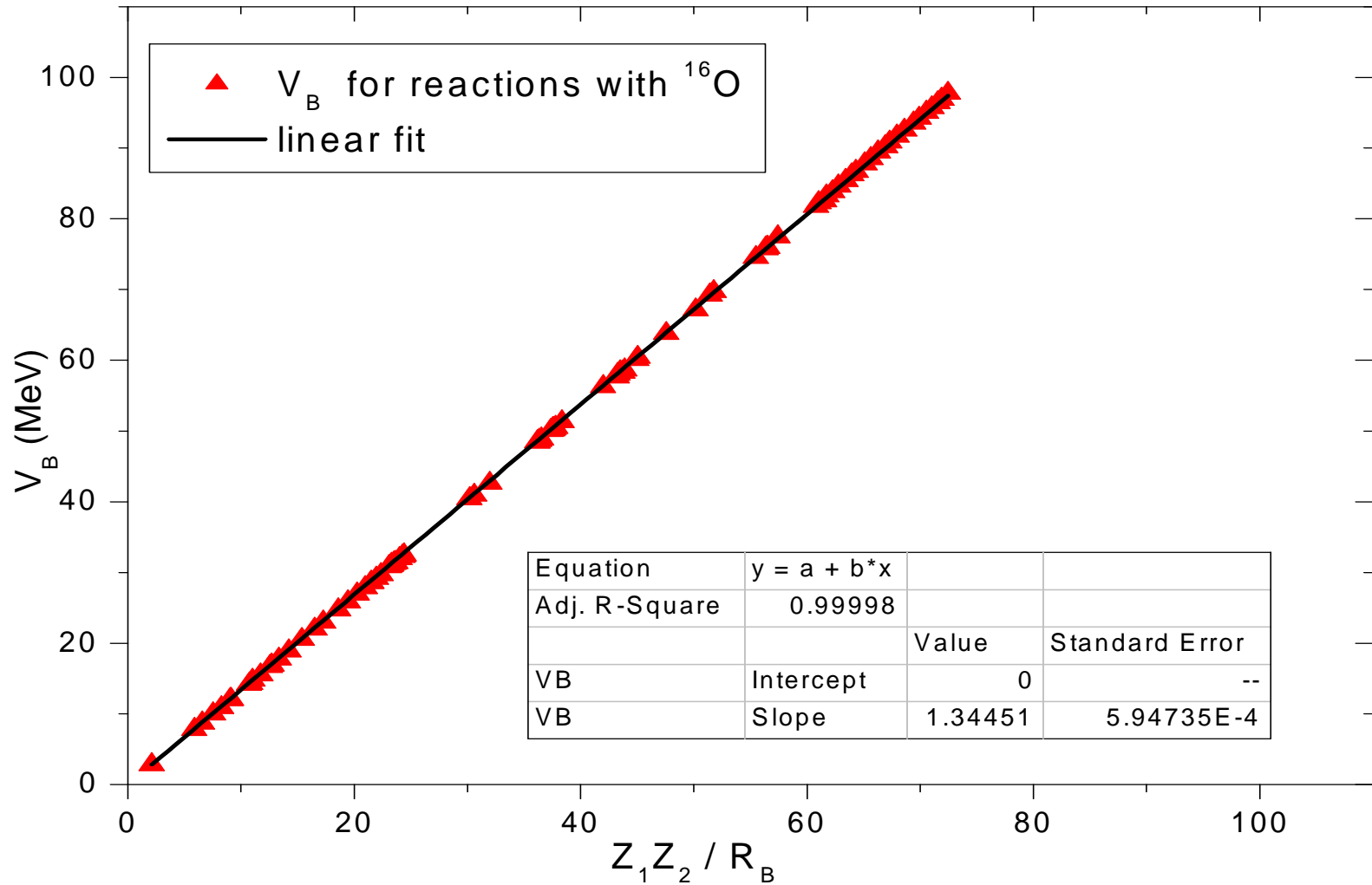


Figure (1.5-b) The same as Figure (1.5-a) but for ^{16}O projectile. The solid line is a linear fit to data and represented by

$$V_B = (1.34451 \pm 5.94735 \times 10^{-4}) \times Z_T Z_P / R_B .$$

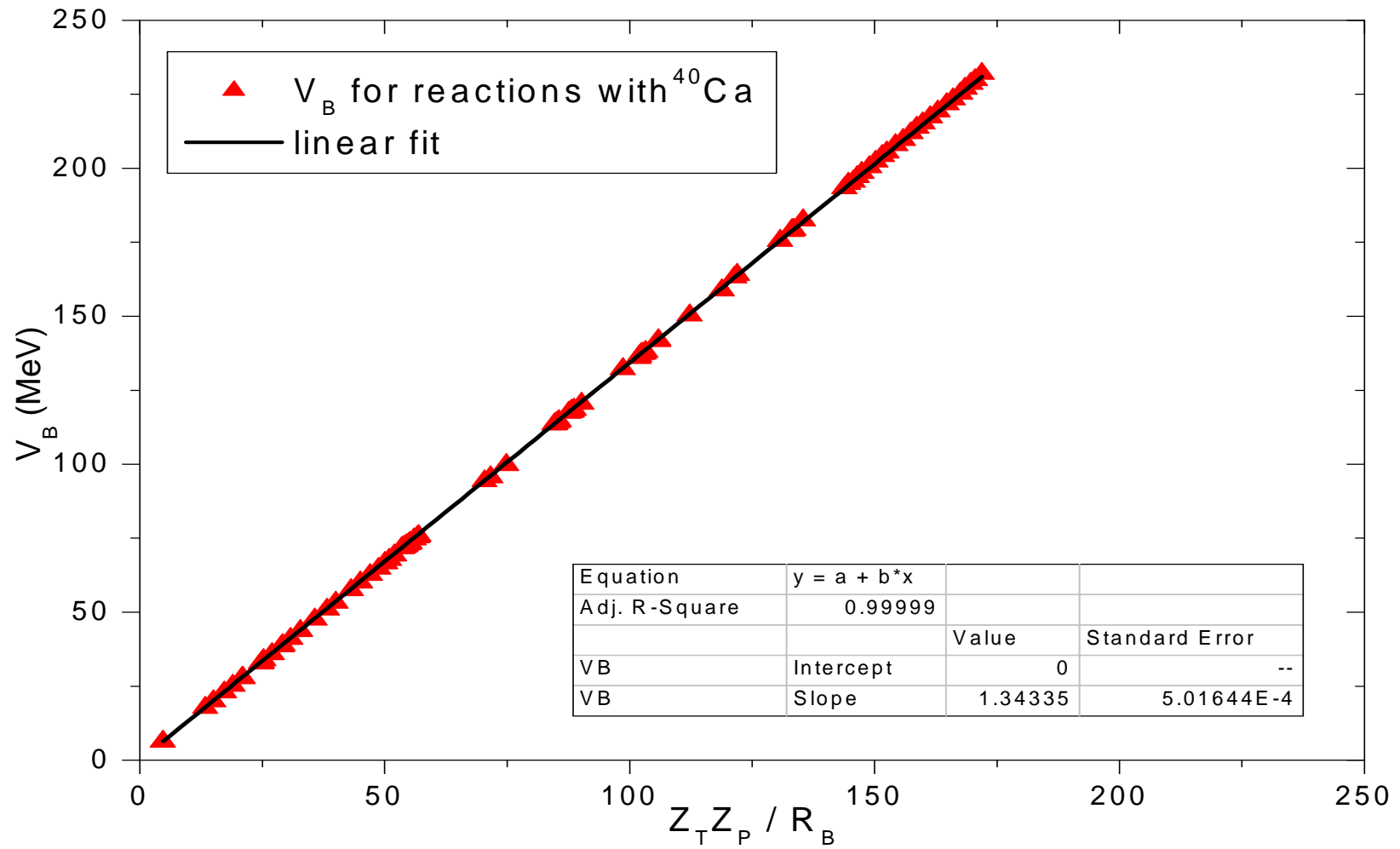


Figure (1.5-c) The same as Figure (1.5-a) but for ^{40}Ca projectile. The solid line is a linear fit to data and represented by

$$V_B = (1.34335 \pm 5.01644 \times 10^{-4}) \times Z_T Z_P / R_B .$$

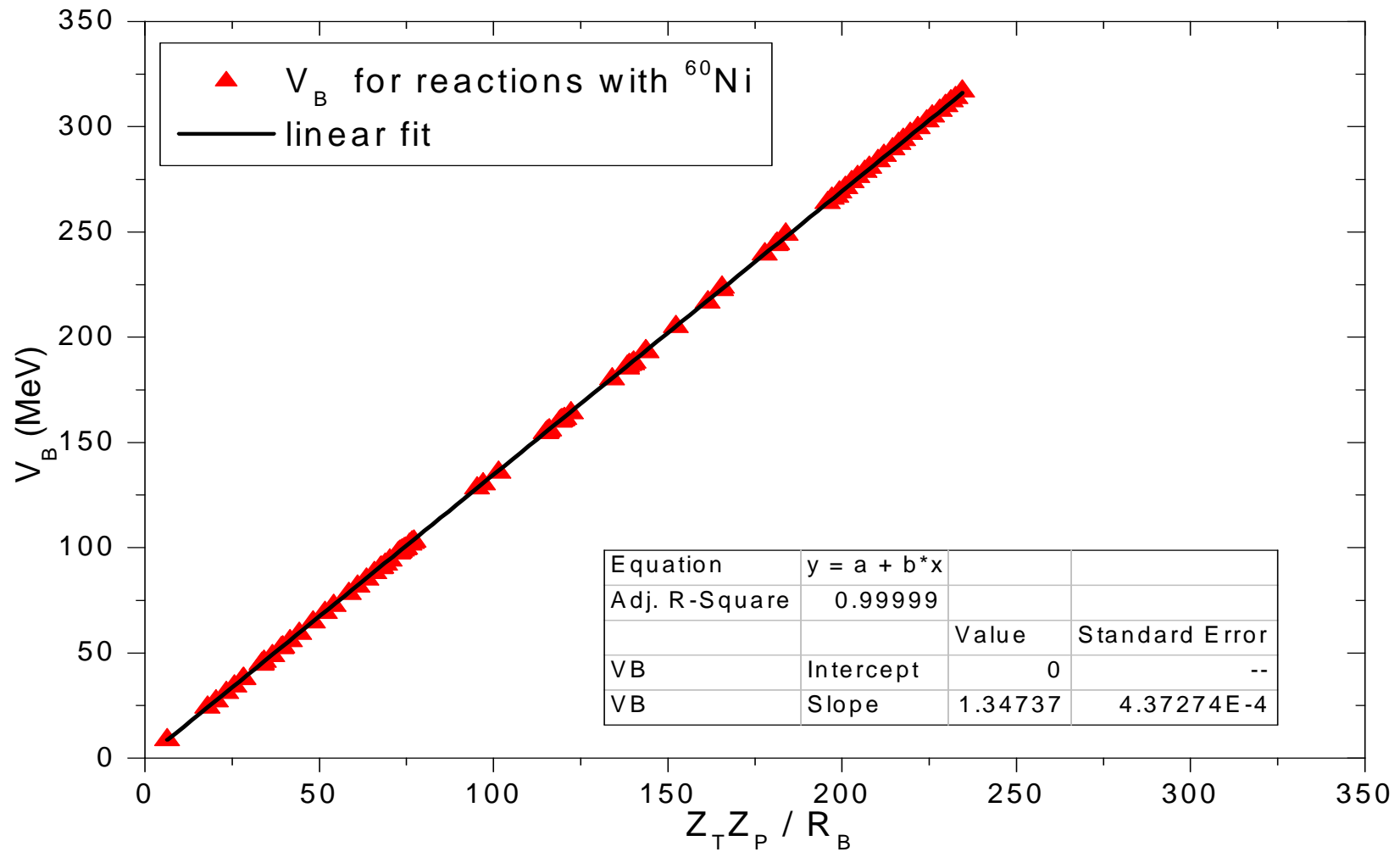


Figure (1.5-*d*) The same as Figure (1.5-*a*) but for ^{60}Ni projectile. The solid line is a linear fit to data and represented by

$$V_B = (1.34737 \pm 4.37274 \times 10^{-4}) \times Z_T Z_P / R_B.$$

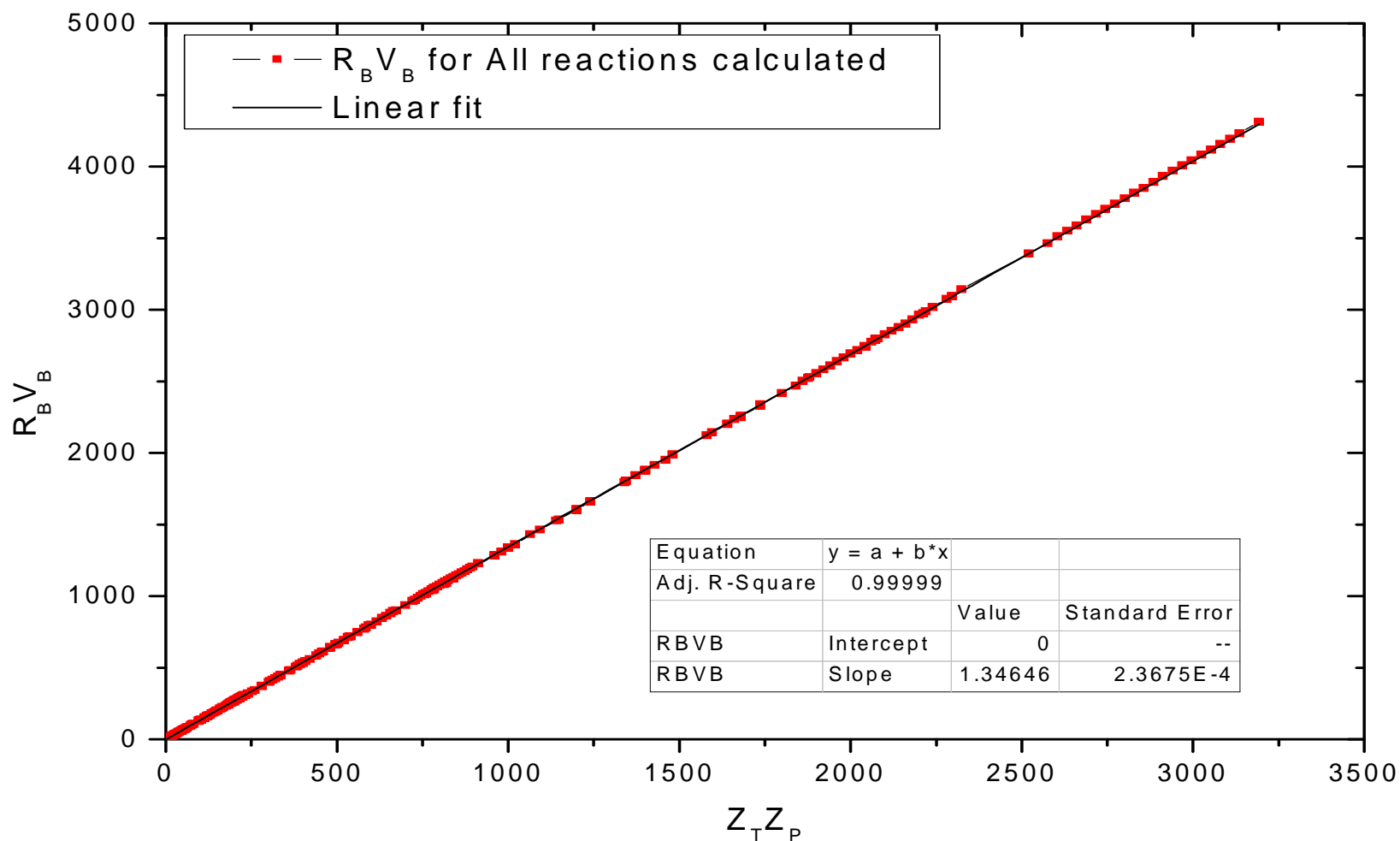


Figure (1.6-a) The behavior of $(R_B V_B)$ product for all reaction done within the present chapter with $Z_T Z_P$. The solid line is a linear fit to data and represented by

$$R_B \times V_B = (1.34646 \pm 2.3675 \times 10^{-4}) \times Z_T Z_P.$$

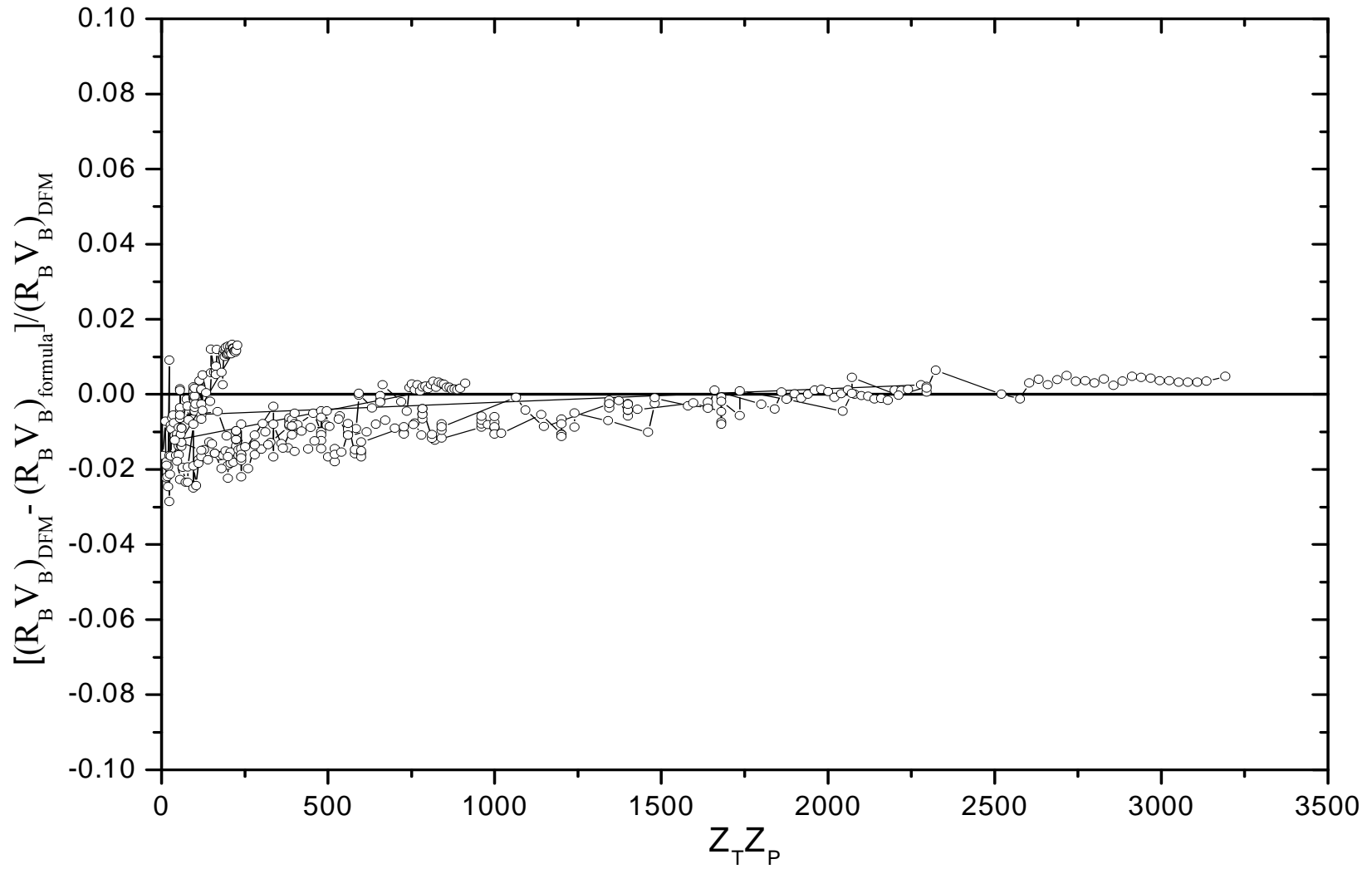


Figure (1.6-b) the relative differences in the values of $R_B V_B$ calculated using DFM and the values calculated using formula (1.13) for all reactions studied in chapter (1).

1.5 Discussion

In the present study of the systematic behaviour of the fusion barrier parameters, we considered ${}^4\text{He}$, ${}^{16}\text{O}$, ${}^{40}\text{Ca}$, and ${}^{60}\text{Ni}$ as projectiles and a large number of different target nuclei. We extended the study to a number of SHE with $Z \leq 114$. The DFM calculations were performed to find the fusion barrier parameters, V_B and R_B , as well as the values of nuclear and Coulomb potentials at $R = R_B$, for reactions of ${}^4\text{He}$, ${}^{16}\text{O}$, ${}^{40}\text{Ca}$, and ${}^{60}\text{Ni}$ with large number of nuclei as given in tables (1.2-*a*, *b*, *c*, and *d*). From the values of V_C and V_N in tables (1.2) it is clear that major contribution to V_B comes from Coulomb potential, and the magnitude of nuclear potential at R_B is less than 8% of the magnitude of Coulomb potential at R_B .

Some values of R_B show unexpected behaviour, for example the reaction between ${}^{16}\text{O}$ and ${}^{25}\text{Mg}$ has value of $R_B = 8.963 \text{ fm}$, while the reaction between ${}^{16}\text{O}$ and ${}^{26}\text{Mg}$ has $R_B = 8.888 \text{ fm}$, in this case the mass number (A) increases, while R_B decreases. Similar behaviour is found for reactions of ${}^{16}\text{O}$ with (${}^{148}\text{Nd}$ and ${}^{150}\text{Nd}$) and (${}^{181}\text{Ta}$, ${}^{184}\text{W}$). This behaviour shows that R_B is not sensitive to the mass only, but also to the density distribution. From table (1.1) and comparing density distribution parameters for the examples

mentioned above we note that the nuclei which have large diffuseness parameters, give unexpected large fusion radii. For ^{25}Mg and ^{26}Mg , the diffuseness values are (0.608 fm) and (0.524 fm) respectively, and ^{181}Ta has diffuseness parameter of 0.64 fm. Moreover, reactions with target nuclei such as ^{186}W and ^{209}Bi , which have relatively small diffuseness parameters, (0.480 fm and 0.468 fm respectively), provide smaller values of R_B than reactions with the lighter nuclei ^{184}W and ^{208}Pb respectively. Large value of diffuseness enhances the attractive nuclear contribution before and at the position of Coulomb barrier, and hence shifts the barrier outwards.

In a first trial we represented R_B as a function of $A_1^{1/3} + A_2^{1/3}$ -as is usually done [51, 54, 55] - but the dependence, in this case, was not regular. More regular dependence of R_B is obtained with the sum of root mean square (rms) radii of interacting nuclei. Figures (1.2-a, b, c, and d) show the variation of R_B parameter with the sum of the calculated rms radii of the interacting nuclei. The rms radius is calculated from the equation

$$\langle r^2 \rangle^{\frac{1}{2}} = \left[\frac{\int_0^\infty \rho(r)r^4 dr}{\int_0^\infty \rho(r)r^2 dr} \right]^{\frac{1}{2}}$$

where $\rho(r)$ is the density distribution of the nucleus described in section (1.3). As shown in figures (1.2-*a*, *b*, *c*, and *d*) the variation of R_B with sum of rms radii of colliding nuclei shows systematic variation with very little spread of data, the straight–line fit of the data in those figures clearly shows the success of first order parameterization of R_B in terms of rms radii. The linear fit in figures (1.2-*a*, *b*, *c*, and *d*) has a general form of

$$R_B = B \left(\langle r_T^2 \rangle^{\frac{1}{2}} + \langle r_P^2 \rangle^{\frac{1}{2}} \right) + C.$$

This is a simple first order expression with two coefficients B and C , the values of the coefficients are given in figures (1.2-*a*, *b*, *c*, and *d*) for reactions of deferent targets with ${}^4\text{He}$, ${}^{16}\text{O}$, ${}^{40}\text{Ca}$, and ${}^{60}\text{Ni}$ respectively. In case of ${}^{40}\text{Ca}$, and ${}^{60}\text{Ni}$ the coefficients are almost equal, $B \cong 1.1$ and $C \cong 2.4 \text{ fm}$. The value of B for the reactions involving ${}^4\text{He}$ is larger than the value mentioned above by about (7.3%) and for the reactions with ${}^{16}\text{O}$ is larger by about (2.4%). The second coefficient R_0 for reactions with ${}^4\text{He}$ has the same value as for ${}^{40}\text{Ca}$, and ${}^{60}\text{Ni}$ but for reactions with ${}^{16}\text{O}$ is smaller by about (3%). Small differences in the values of B and R_0 for reactions with light nuclei prove the possibility of using a single mathematical expression

for the potential barrier position (R_B) between heavy ion (HI) pairs with high accuracy. So that, the expression of R_B becomes,

$$R_B = 1.1 \left(\langle r_T^2 \rangle^{\frac{1}{2}} + \langle r_P^2 \rangle^{\frac{1}{2}} \right) + 2.4, \quad (1.12)$$

this expression gives a simple and direct method to calculate the potential barrier radius (R_B) at least for large number of HI reactions from the knowledge of rms radii of reaction pair. The accuracy of the above formula is tested by comparing the values of R_B calculated using DFM and the values calculated using formula (1.12), the differences in values are shown in figure (1.3-a) for the reactions with ${}^4\text{He}$, ${}^{16}\text{O}$, ${}^{40}\text{Ca}$, and ${}^{60}\text{Ni}$. For the reactions with ${}^{40}\text{Ca}$, and ${}^{60}\text{Ni}$ all deviations are located between the two horizontal lines - 0.08 *fm* and 0.09 *fm* and then the values of R_B for these reactions can be calculated using the above formula within about 0.1 *fm*. Deviations for reactions with ${}^{16}\text{O}$ reach to 0.22 *fm* and for reactions with ${}^4\text{He}$ reach to 0.72 *fm*. Deviations for reactions with ${}^4\text{He}$ is unacceptable because of thier large values, and because of location of all deviations above 0.3 *fm* *i.e.* the most accurate result has an error of 0.3 *fm*. Figure (1.3-b) is the same as Figure (1.3-a) but R_B is calculated using a separate formula, other than equation (1.12), obtained for reactions of ${}^4\text{He}$ with deferent targets. This formula is

$$R_B = 1.18075 \left(\langle r_T^2 \rangle^{\frac{1}{2}} + \langle r_P^2 \rangle^{\frac{1}{2}} \right) + 2.40683$$

In this case the deviations are well distributed around the zero deviation line, and all deviations are located between the two horizontal lines -0.15 fm and 0.12 fm . Thus, equation (1.12) can be used satisfactory for reactions involving projectiles of mass numbers $A_p \geq 16$, while for ${}^4\text{He}$ as projectile, R_B can be obtained from the formula mentioned above.

As mentioned before, the major contribution to V_B comes from Coulomb potential, so one can predict strong dependence of V_B on relevant quantities such as $Z_T Z_P / [A_T^{1/3} + A_P^{1/3}]$ or $Z_T Z_P / [\langle r_T^2 \rangle^{\frac{1}{2}} + \langle r_P^2 \rangle^{\frac{1}{2}}]$. Authors in reference [56] have suggested a parameterization of V_B for light colliding nuclei with mass numbers up to 64, as a second order function of $Z_T Z_P / [A_T^{1/3} + A_P^{1/3}]$ as

$$V_B = (0.845 \pm 0.02) \frac{Z_T Z_P}{A_T^{1/3} + A_P^{1/3}} + (1.3 \pm 0.25) \times 10^{-3} \left[\frac{Z_T Z_P}{A_T^{1/3} + A_P^{1/3}} \right]^2.$$

In fact this expression is simple and direct, but it is not general for all nuclei or needs to be generalized. In order to obtain similar general expression, figures (1.4-a, b, c, and d) show the variation of calculated

barrier height (V_B) with the quantity $Z_T Z_P / [A_T^{1/3} + A_P^{1/3}]$, for reactions with projectiles ${}^4\text{He}$, ${}^{16}\text{O}$, ${}^{40}\text{Ca}$, and ${}^{60}\text{Ni}$ respectively and the results are fitted to a polynomial of degree two with no zero order term to get an expression similar to the one mentioned above. It is important to note that fits in figures (1.4-*a*, *b*, *c*, and *d*) are restricted to pass through the origin *i.e.* the zero order term is restricted to be zero. Without this restriction, fits will contain a negative zero order term which leads to unphysical result of negative barrier height. Figures (1.4-*a*, *b*, *c*, and *d*) show systematic variation with very little spread of points, and each graph can accurately represented by the expression obtained by fitting the data points. The four expressions obtained for reactions of different nuclei with ${}^4\text{He}$, ${}^{16}\text{O}$, ${}^{40}\text{Ca}$, and ${}^{60}\text{Ni}$ are similar but the coefficients are not equal. The differences between the coefficients for different projectiles can not be neglected. The coefficients of the first order terms are 0.74999, 0.8529, 0.91656, and 0.95546 for reactions with ${}^4\text{He}$, ${}^{16}\text{O}$, ${}^{40}\text{Ca}$, and ${}^{60}\text{Ni}$ respectively; it is clear that the values of this coefficient increase with irregular step and do not oscillate around a mean value as obtained in the parameterization of R_B mentioned before. The coefficients of the second order terms are very small in magnitude compared to the coefficients of the first order terms but their values decrease in very large

steps from figure (1.4-*a*) to figure (1.4-*d*). Comparisons between the four formulae show that it will not be easy to suggest one simple and general formula for V_B as a function of $Z_T Z_P / [A_T^{1/3} + A_P^{1/3}]$.

The previous discussion shows the systematic dependence of the potential barrier parameters on some structural quantities of the interacting nuclei. Now, it is logical to discuss the relation - if it exists - between the potential barrier parameters each other. In normal or even extreme conditions, charge number (Z) and mass number (A) can not exceed definite regions of stability on the A - Z plane, this fact supports the idea of systematic Interdependent variation of the potential barrier parameters, because the regular increase of Z with A indicates a regular growing of both repulsive and attractive fields of the nucleus. Figures (1.5-*a*, *b*, *c*, and *d*) show the variation of calculated barrier height (V_B) with $(Z_T Z_P / R_B)$ for reactions with ${}^4\text{He}$, ${}^{16}\text{O}$, ${}^{40}\text{Ca}$, and ${}^{60}\text{Ni}$ respectively, and the results of linear fit to data, the graphs show very little scatter of data, moreover, the values of coefficients of the resulting linear fits are close to each other, and an average coefficient may be deduced to find a relation between the potential barrier parameters (V_B and R_B) as “*the product of the potential barrier parameters (V_B and R_B) is directly proportional to $Z_T Z_P$* ”, this relation can be stated symbolically as

$$R_B \times V_B = C \times Z_T Z_P,$$

where the constant of proportionality (C) is the same as the coefficient of resulting linear fit in figures (1.5-*a*, *b*, *c*, and *d*), and has a value around 1.345. This behavior is illustrated in figure (1.6-*a*) for all calculated parameters in the present chapter, and the least squares linear fit gives

$$R_B \times V_B = (1.34646 \pm 2.3675 \times 10^{-4}) \times Z_T Z_P. \quad (1.13)$$

The accuracy of the above formula is tested in figure (1.6-*b*) by comparing the product of $R_B V_B$ calculated using DFM and the values calculated using formula (1.13). The differences shown in figure (1.6-*b*) do not exceed 2%, except for a number of reactions between ${}^4\text{He}$ and some nuclei, reach to about 3%. In general, the accuracy of this formula is higher than 98% for all heavy and super heavy ion reactions. The above relation can efficiently used to calculate the potential barrier parameters, if an accurate method is valid to calculate one of them.

References

- [1] M. Ismail, W. M. Seif, M. M. Osman, H. El-Gebaly, and N. M. Hassan, *Phys. Rev. C* 72 (2005) 064616.
- [2] H. Feshbach, *Theoretical Nuclear Physics* (Wiley, New York, 1992).
- [3] D.M. Brink and F. Stancu, *Nucl. Phys. A* 243 (1975) 175.
- [4] Farid M. El-Azab and G.R. Satchler *Nucl. Phys. A* 438 (1985) 525.
- [5] G.R. Satchler and W.G. Love *Phys. Rep.* 55 (1979)183.
- [6] J. Blocki, J. Randrup, W.J. Swiatecki, and C.F. Tsang, *Ann. Phys. (NY)* 105 (1977) 427.
- [7] H. Gauvin, Y. LeBeyce, M. Lefort, and C. deprun, *Phys. Rev. Lett.* 28 (1972) 697.
- [8] M.K. Pal, *Theory of Nuclear Structure* (New Delhi-Madras: Affiliated East-West Press PVT) (1982).
- [9] J.M. Irvine, *Nuclear Structure Theory* (Oxford: Pergamon, 1972).
- [10] P.E. Hodgson, *Nuclear Reactions and Nuclear Structure* (Oxford: Clarendon, 1971).
- [11] A. Bohr and B. Mottelson, *Nuclear Structure* (New York: Benjamin,1969).
- [12] C. Mahaux, K.T.R. Davies and G.R. Satchler, *Phys. Rep.* 224 (1993) 237.
- [13] C. Mahaux and R. Sartor, *Adv. Nucl. Phys.* 20 (1991) 1.
- [14] M.S. Hussein and K.W. McVoy, *Prog. Part. Nucl. Phys.* 12 (1984) 103.
- [15] G.R. Satchler, *Direct Nuclear Reactions* (Oxford Univ. Press, Oxford, 1983).
- [16] C. Mahaux, *Microscopic Optical Potentials* (Springer, Berlin, 1979) p. 1.
- [17] G.W. Greenlees, W. Makofske and G.J. Pyle, *Phys. Rev. C* 1 (1970) 1145.

- [18] G.W. Greenlees, G.J. Pyle and Y.C. Tang, *Phys. Rev.* 171 (1968) 1115.
- [19] N. Vinh Mau, *Phys. Lett. B* 71 (1977) 5.
- [20] B. Sinha, *Phys. Rev. Lett.* 33 (1974) 600; *Phys. Rev. C* 11 (1975) 1546.
- [21] G.R. Satchler, in: *Proc. int. Conf. on Reactions between Complex Nuclei*, Nashville, Tenn., 1974 (North-Holland Publishing Co., Amsterdam, 1974).
- [22] C.B. Dover and J.P. Vary, *Phys. Rev. Lett.* 31(1973)1510.
- [23] M.E. Brandan, G.R. Satchler, *Physics Reports* 285 (1997) 143.
- [24] H. Feshbach, *Theoretical Nuclear Physics* (Wiley, New York, 1992).
- [25] K.A. Gridnev, E.E. Rodionova, S.N. Fadeev, *Physics of Atomic Nuclei*, Vol. 71, No.7 (2008) 1262.
- [26] S. Szilner, W. von Oertzen, Z. Basrak, F. Haas, and M. Milin, *Eur. Phys. J. A* 13, (2002) 273.
- [27] Dao T. Khoa, W. von Oertzen and H.G. Bohlen, *Phys. Rev. C* 49 (1994) 1652.
- [28] M.E. Brandan and A. Menchaca-Rocha, *Phys. Rev. C* 23 (1981) 1272.
- [29] R.G. Stokstad, R.M. Wieland, G.R. Satchler, C.B. Fulmer, D.C. Hensley, S. Raman, L.D. Rickertsen, A.H. Snell and P.H. Stelson, *Phys. Rev. C* 20 (1979) 655.
- [30] R.M. Wieland, R.G. Stokstad, G.R. Satchler and L.D. Rickertsen, *Phys. Rev. Lett.* 37 (1976) 1458.
- [31] M.E. Brandan and G.R. Satchler, *Phys. Lett. B* 256 (1991) 311.
- [32] W.G. Love, *Phys. Lett. B* 72 (1977) 4.
- [33] P. Ring and P. Schuck (Springer-Verlag, 1980).
- [34] D.J. Rowe, *Nuclear Collective Motion: Models and Theory* (Methuen, London ,1970)

- [35] T.H.R. Skyrme, Nucl. Phys. 9 (1959) 615.
- [36] C.W. De Jager, H. De Vries, C. De Vries, Atomic Data And Nuclear Data Tables 14 (1974) 479.
- [37] M. Ismail, H. Abou-Shady, W. M. Seif and A. Bakry, Physics of Atomic Nuclei, Vol. 69 (2006) 1463.
- [38] G.R. Satchler, Phys. Lett. B 59 (1975) 121.
- [39] G. Bertsch, J. Borysowicz, H. McManus and W.G. Love, Nucl. Phys. A 284 (1977) 399.
- [40] R. Reid, Ann. Phys. 50 (1968) 411.
- [41] M. Lacombe, B. Loiseau, J.M. Richard, R. Vinh Mau, J. Cote, P. Pires and R. de Tournreil, Phys. Rev. C 21 (1980) 861.
- [42] D.T. Khoa, G.R. Satchler and W. von Oertzen, Phys. Rev. C 56 (1997) 954.
- [43] D.T. Khoa, W. von Oertzen and A.A. Ogloblin, NPA 602 (1996) 98.
- [44] Zhang Gao-Long et al, Chinese Phys. B 18 (2009) 136.
- [45] K. Hagino, T. Takehi, and N. Takigawa, Phys. Rev. C 74 (2006) 037601.
- [46] M. Ismail, A. Sh. Ghazal and H. Abu-Zahra J. Phys. G: Nucl. Part. Phys. 25 (1999) 2137.
- [47] N. Vinh Mau, Nucl. Phys. A 457 (1986) 413.
- [48] W. J. Swiatecki, K. Siwek-Wilczynska and J. Wilczynski (Concepts of Physics, Vol. V, No. 4, 2008)
- [49] Yu. Ts. Oganessian, V. K. Utyonkov, Yu. V. Lobanov, et al., Phys. Rev. C 70 (2004) 064609.
- [50] M.G. Itkis, Yu. Ts. Oganessian, and V.I. Zagrebaev, Phys. Rev. C 65 (2002) 044602.

- [51] R.A. Broglia and A. Winther, Heavy-Ion Reactions Lecture Notes (Redwood City, CA: Addison-Wesley, 1981) p 116.
- [52] P.J. Moffa, C.B. Dover and J.P. Vary, Phys. Rev. C16 (1977) 1857.
- [53] M. Ismail, M. Rashdan, Amand Faessler, M. Trefz and H. Mansour, Z. Phys. A 323 (1986) 399.
- [54] Basudeb Sahu and C.S. Shastry J. Phys. G: Nucl. Part. Phys. 25 (1999) 1909.
- [55] N.G. Nicolis Eur. Phys. J. A 21 (2004) 265.
- [56] Rajeev K. Puri and Raj K. Gupta, Phys. Rev. C45 (1992) 1837.

Chapter 2

*Universal function of nuclear proximity
potential derived from M3Y nucleon-
nucleon interaction*

Chapter 2

Universal function of nuclear proximity potential derived from M3Y nucleon-nucleon interaction

2.1 Introduction

Recently, the study of nuclear fusion has been of much interest, and the knowledge of the barrier parameters is also known to be important for fusion studies. Well knowledge of the barrier parameters (barrier height and position) helps to choose the optimum conditions for fusion to give the wanted results. The height of the barrier is especially important for the production of heavy and superheavy elements (SHE) [1]. In chapter (1), study of barrier parameters has been performed in the frame work of DFM, starting from empirical nuclear densities and M3Y nucleon-nucleon (NN) force. Systematic behavior of the fusion barrier parameters has been presented for large number of interacting ion pairs, and we discussed

analytical expressions for calculation of the interaction barrier directly, starting from masses, charges, and/or radii of interacting nuclei.

Evaluation of nucleus-nucleus potential is a complicated problem, especially when the ground states of interacting nuclei are deformed [2- 4]. The nuclear part of a nucleus-nucleus potential has been studied in the framework of various models [5- 15]. The so-called “proximity” model [12, 15, 16] can easily and successfully be used to calculate the nuclear interaction between two medium-heavy or heavy nuclei. The original proximity interaction derived by Blocki et al [16] was obtained from a description of the interacting nuclei by the Thomas-Fermi approximation of the energy density of the ion-ion system. The expression of proximity interaction for spherical nuclei is given as

$$V_p(s_0) = 4\pi\bar{R}b\gamma\Phi(s_0) \quad (2.1)$$

The nuclear proximity potential, given above, is the product of two factors, one depending on the shape and geometry of the two nuclei ($\bar{R}b\gamma$), and the other is the universal function depending only on the shortest separation distance between them ($\Phi(s_0)$). In the first factor, b is the diffuseness of the nuclear surface, given by

$$b = \frac{\pi}{2\sqrt{3} \ln 9} \times t_{10-90} \quad (2.2);$$

where t_{10-90} is the thickness of the surface in which the nuclear matter density profile changes from 90% to 10%. For a 2pF distribution, t_{10-90} is related to the diffuseness parameter a through: $t_{10-90} = 2a \ln 9$, this give,

$$b = \frac{\pi}{\sqrt{3}} \times a$$

Many authors [16- 19] use a constant value of 1 *fm* or 0.99 *fm* as an approximate value of b for heavy ion reactions. Any way, we will use the formula (2.2) to calculate the surface width (b) for any system, whatever the shape of density distribution. The diffused surface width for any reaction pair is taken as the mathematical average of the values obtained for each nucleus individually. γ is the specific nuclear surface energy, given by

$$\gamma = 0.9517 \left[1 - 1.7826 \left(\frac{N - Z}{A} \right)^2 \right] \text{MeV fm}^{-2} \quad (2.3);$$

where N , Z and A are respectively the neutron, charge, and mass numbers of the bulk reaction system, *i.e.* for the reaction between two ions donated by 1 and 2,

$$\begin{aligned}
 N &= N_1 + N_2 \\
 Z &= Z_1 + Z_2 ; \\
 A &= A_1 + A_2
 \end{aligned}$$

\bar{R} is the mean curvature radius of the reaction pair, given by

$$\bar{R} = \frac{R_1 R_2}{R_1 + R_2} \quad (2.4);$$

where R_1 and R_2 are the radii of the two interacting nuclei.

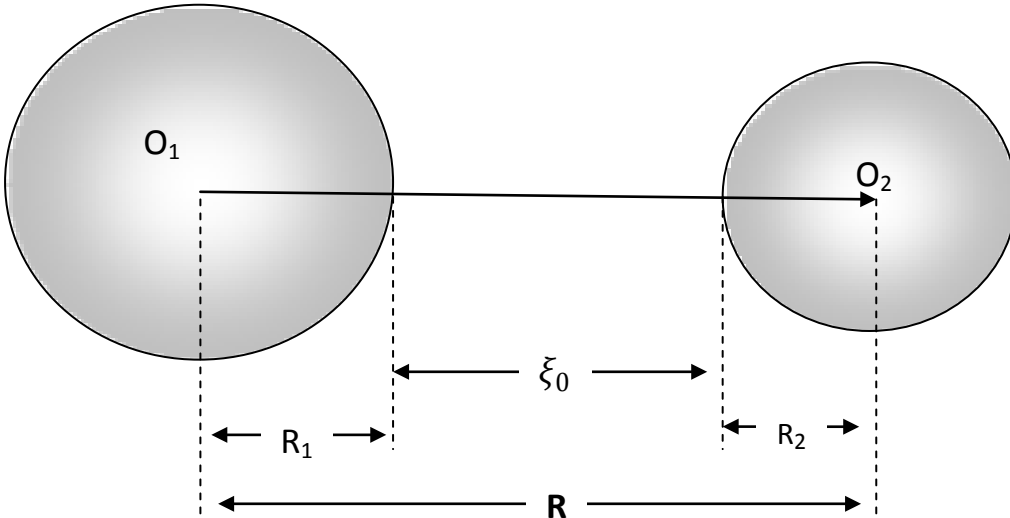


Figure (2.1)

The minimum separation distance between the nuclear surfaces is the essential quantity of the idea of proximity [16]. Figure (2.1) shows the minimum separation distance (ξ_0) between the nuclear surfaces for interaction between two spherical nuclei, the dimensionless minimum

separation distance (s_0) is the minimum separation distance (ξ_0) defined in units of b , i.e. $s_0 = \xi_0/b$. For the reactions between deformed and oriented nuclei the problem becomes complicated and calculation of s_0 can be done by using sophisticated iterative procedures just like introduced in references [12, 15].

The second factor in Equation (2.1) is the universal function $\Phi(s_0)$, independent of the shapes of nuclei or the geometry of nuclear system, but depends on the minimum separation distance s_0 ; it is therefore one function for all nuclei. The main advantage of the proximity potential is in the idea of universality (or system-independence). Authors in reference [16] (and references there) gave a rough approximation of the universal function $\Phi(s_0)$ by the following ‘‘cubic-exponential’’ pocket formula

$$\Phi(s_0) = \begin{cases} -\frac{1}{2}(s_0 - 2.54)^2 - 0.0852(s_0 - 2.54)^3, & s_0 \leq 1.2511 \\ -3.437 \exp\left(-\frac{s_0}{0.75}\right), & s_0 \geq 1.2511 \end{cases} \quad (2.5)$$

The equations mentioned above give only average estimates for doubly closed shell spherical-spherical ion interactions. Variations caused by shell effects and including deformations have to be taken into account. In particular, when using the proximity potential for deformed nuclei, the

minimum separation distance s_0 as well as the mean curvature radius \bar{R} , have to be carefully related to the orientations and shapes of the nuclei. Recently, many studies have been done to derive the proximity potential between two deformed and oriented nuclei [3, 12, 15].

For various applications it is useful to have a simple analytical representation of the universal function which enters in the nucleus-nucleus proximity potential calculation; and it is more useful if that analytical representation agrees with the exact values for large number of interactions. For this purpose, we will use the DFM calculations, which have good agreement with experimental data [20], to give approximate representation of the universal function. It should be noted that the universal function had been derived from HI optical potential calculated from the two colliding nuclear matter approach [21-23]. Recently another shape of the universal function had been obtained from the Skyrme nucleus–nucleus interaction in the semi-classical extended Thomas–Fermi (ETF) approach [24, 25].

In the present chapter we are looking for a universal function of nuclear proximity potential derived from M3Y NN interaction in the framework of DFM, which already considered in chapter (1) of the present thesis.

Since the folding model has its greatest validity in the tail of the potential at which the Thomas–Fermi method breaks down, the calculation of the universal function will be obtained from the DFM as a standard.

The objective of the present work is to make the study of the fusion barrier parameters easier and does not need to complicated numerical calculations as those exist in DFM calculations. This is achieved by deriving a universal function from the DFM considered in the first chapter. The derived universal function must have its greatest validity around the barrier position. For all reactions considered in chapter (1), we calculated the values of s_0 corresponding to the coulomb barrier radii, and we found that the values of s_0 are positive and located between 1 and 4. Thus the success of the obtained universal function in this study depends on the unique value of $\Phi(s_0)$ in that region.

2.2 Calculation of universal function starting from M3Y-Reid NN interaction

It is shown in section (1.2) that the nucleus-nucleus potential is a function of the center of mass separation distance (R) between the two interacting nuclei, and for spherical-spherical interacting pair interaction, it

can be easily calculated by the integral (1.6). For spherical-spherical pair, the minimum separation distance between surfaces of the two nuclei is the distance between the nuclear surfaces along the line connecting the mass centers (R), as shown in figure (2.1), so, the minimum separation distance ξ_0 is defined as

$$\xi_0(fm) = R(fm) - R_1(fm) - R_2(fm)$$

and then, the dimensionless quantity s_0 is

$$s_0 = \frac{\xi_0}{b} = \frac{R - R_1 - R_2}{b} \quad (2.6)$$

The proximity potential $V_P(s_0)$ at any distance must be equal to the value calculated through the DFM with M3Y-interaction ($V_{M3Y}(R)$), and then

$$V_P(s_0) = V_{M3Y}(s_0 b + R_1 + R_2) \quad (2.7)$$

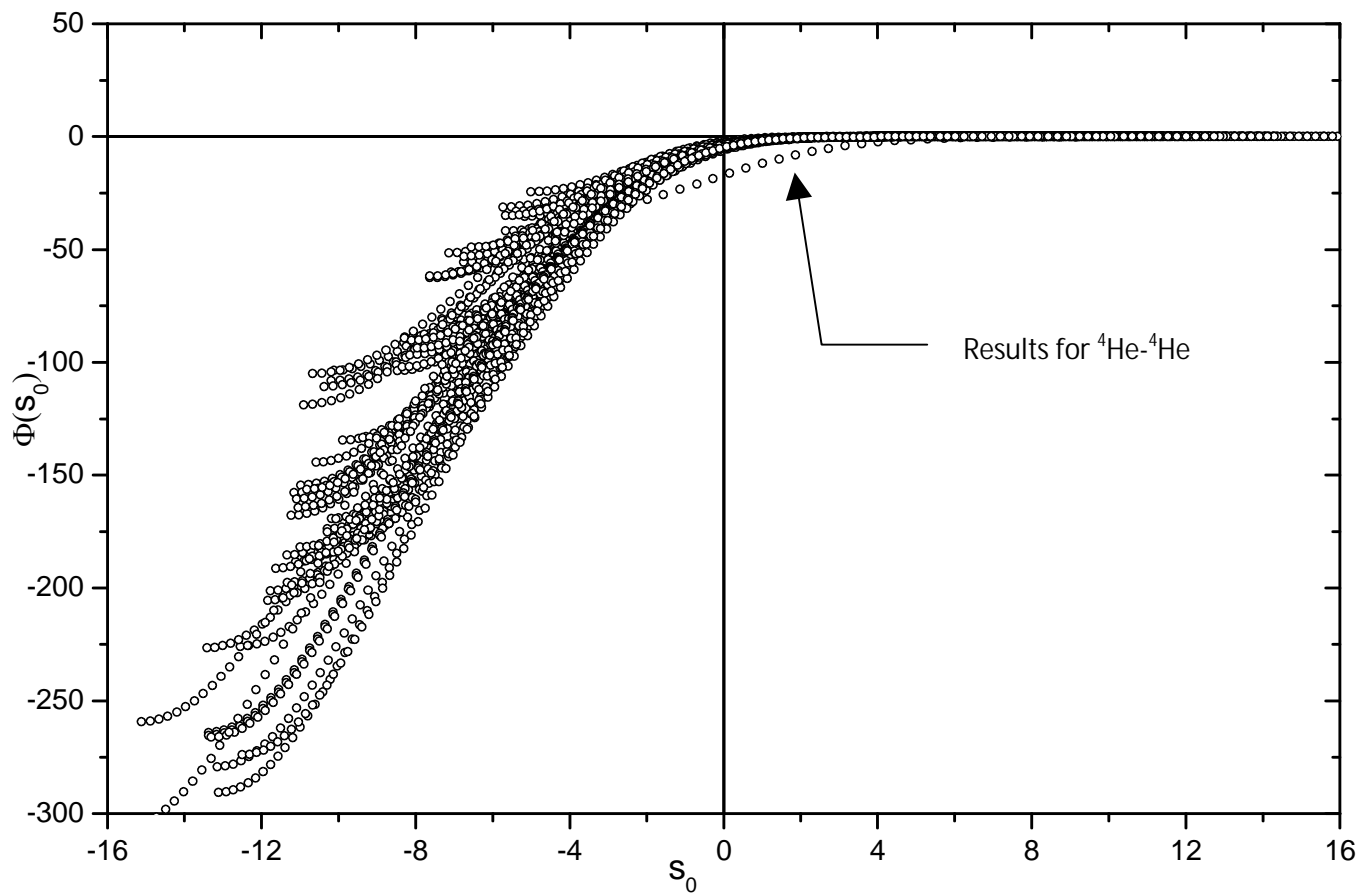
V_{M3Y} in this equation is the nuclear part of nucleus-nucleus potential calculated in the frame work of DFM discussed in section (1.2), the effective nucleon-nucleon interaction used is the well-known M3Y-Reid force [26, 27] in the form given by equation (1.7). The universal function for M3Y NN interaction can be obtained by using the definition of proximity potential

given by equation (2.7) in the original proximity formula (2.1), this give the universal function as

$$\Phi(s_0) = \frac{V_{M3Y}(s_0 b + R_1 + R_2)}{4\pi\bar{R}b\gamma} \quad (2.8)$$

Equation (2.8) defines the universal function for negative, zero, and positive values of s_0 , however, the proximity model becomes less correct as the overlap of the two nuclei increases. This deviation may be a sign of more complex behavior of the nucleus–nucleus potential at small distances in the region of overlap of nuclear surfaces. For large overlaps the nuclear potential will be composed of an energy associated with the bulk of the overlap region, and of surface-layer energy. The proximity model considers only surface-layer interaction, but the DFM gives an average of the effective nucleon–nucleon potential over nuclear densities, and the effects due to nuclear-surface region are automatically taken into account. Therefore the universal function $\Phi(s_0)$, calculated from DFM results, can be approximated to one accurate expression only at the surface and beyond the overlap region at which the surface effect dominates. So, we extend our search for universal function for positive s_0 and around ($s_0 = 0$). In the following Figures we show the universal function calculated by equation (2.8) as a function of s_0 ,

for reactions involving nuclei of mass numbers from 4 to 238. The results involved here are for symmetric reactions only, i.e., reactions between two identical ions. The reason of this choice will be discussed in details in the next section. Reactions involving ${}^4\text{He}$ will be discussed separately, because of its special effect on the calculated universal function. In the present chapter, we will introduce a universal function which is useful for barrier calculation for heavy ion reactions, and a similar universal function for reactions involving ${}^4\text{He}$.



Figure(2.2-a) Universal function $\Phi(s_0)$ calculated from DFM with M3Y interaction as a function of the dimensionless separation s_0 , for symmetric reactions between ions of mass numbers up to 238.

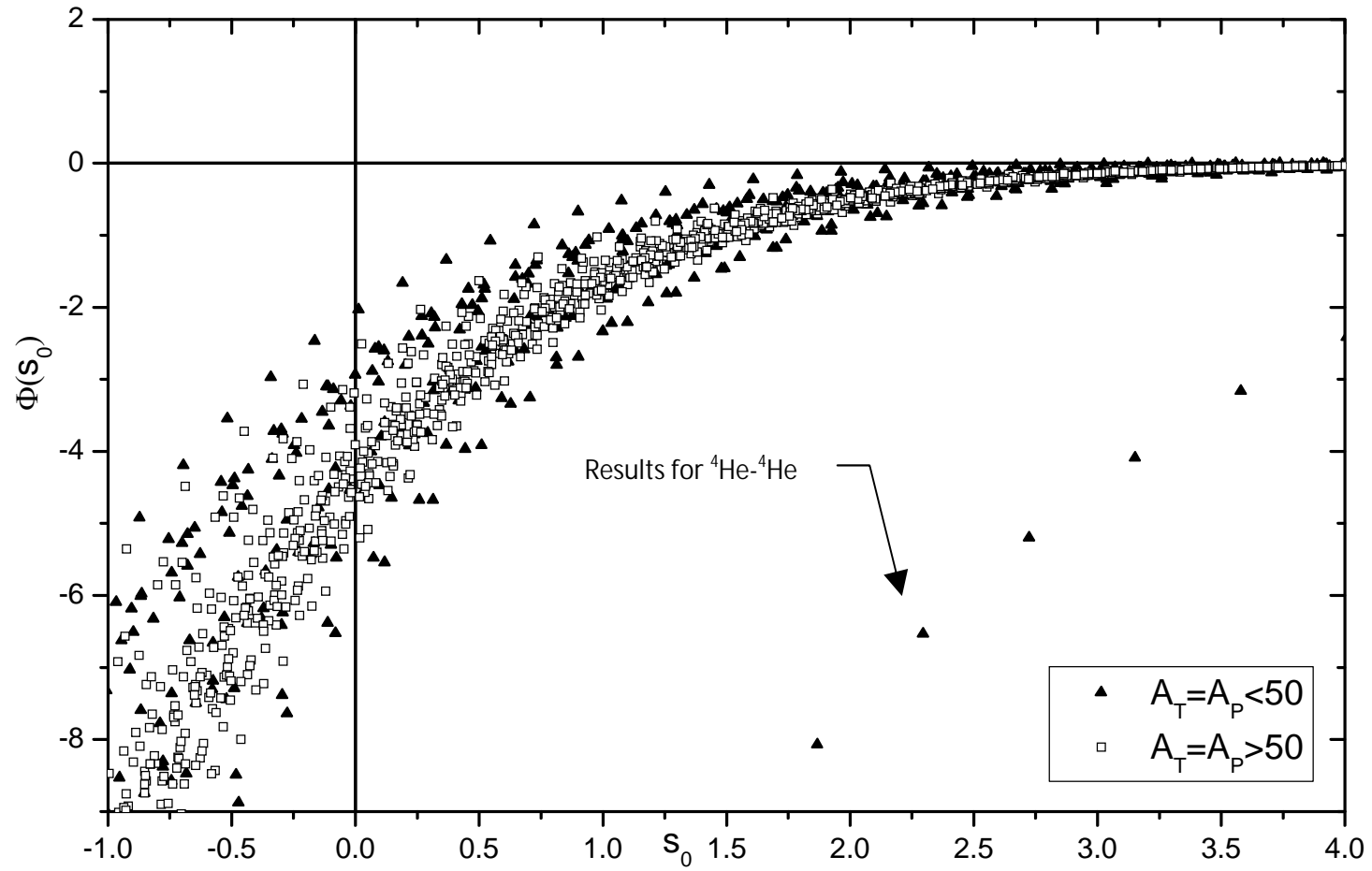


Figure (2.2-*b*) The same as Figure (2.2-*a*) but with s_0 varying in the range $[-1, 4]$

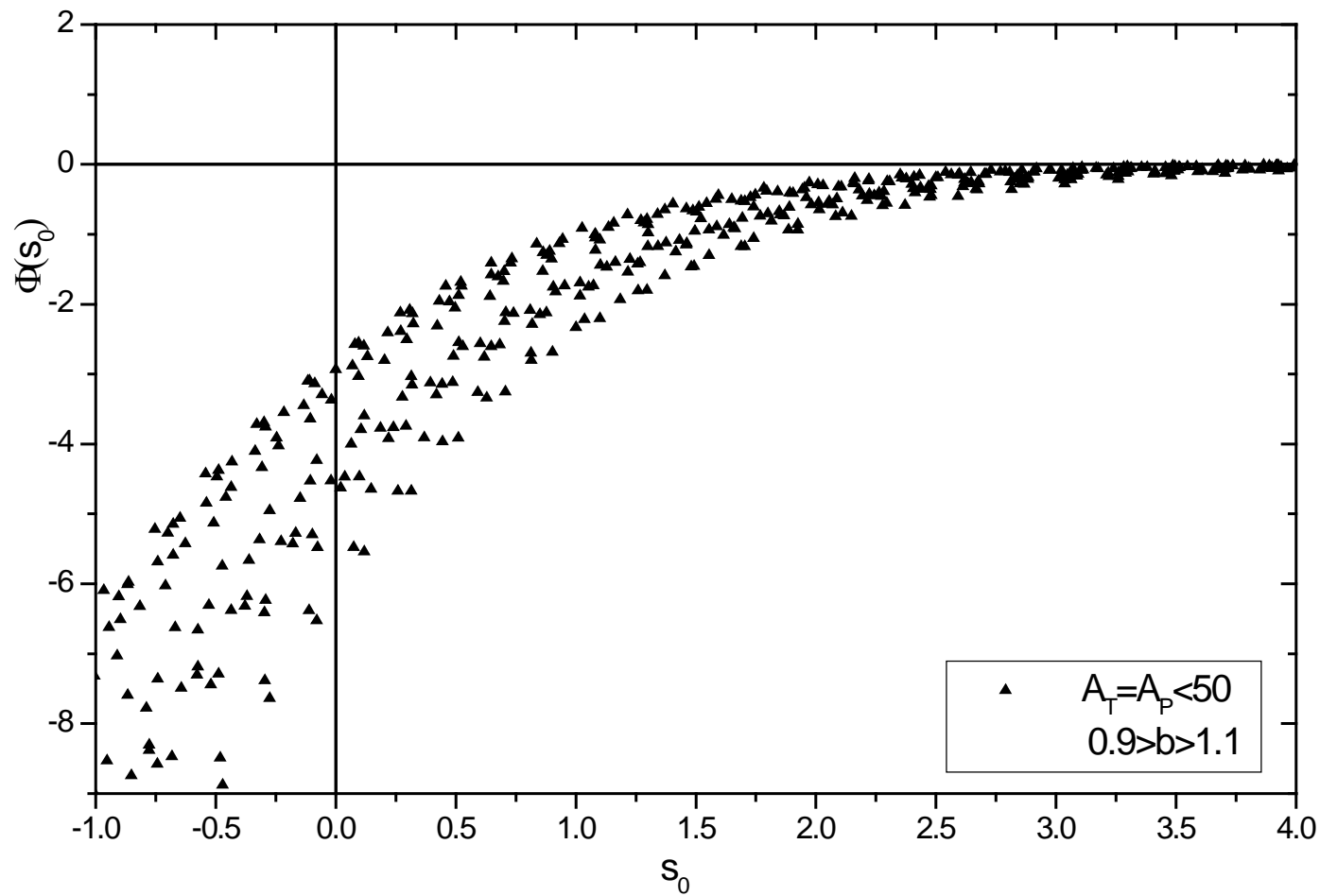


Figure (2.3-a) Calculated universal function $\Phi(s_0)$ as a function of the dimensionless separation s_0 , for reactions involve ions of mass numbers up to 50, and surface diffuseness between 0.9 and 1.1.

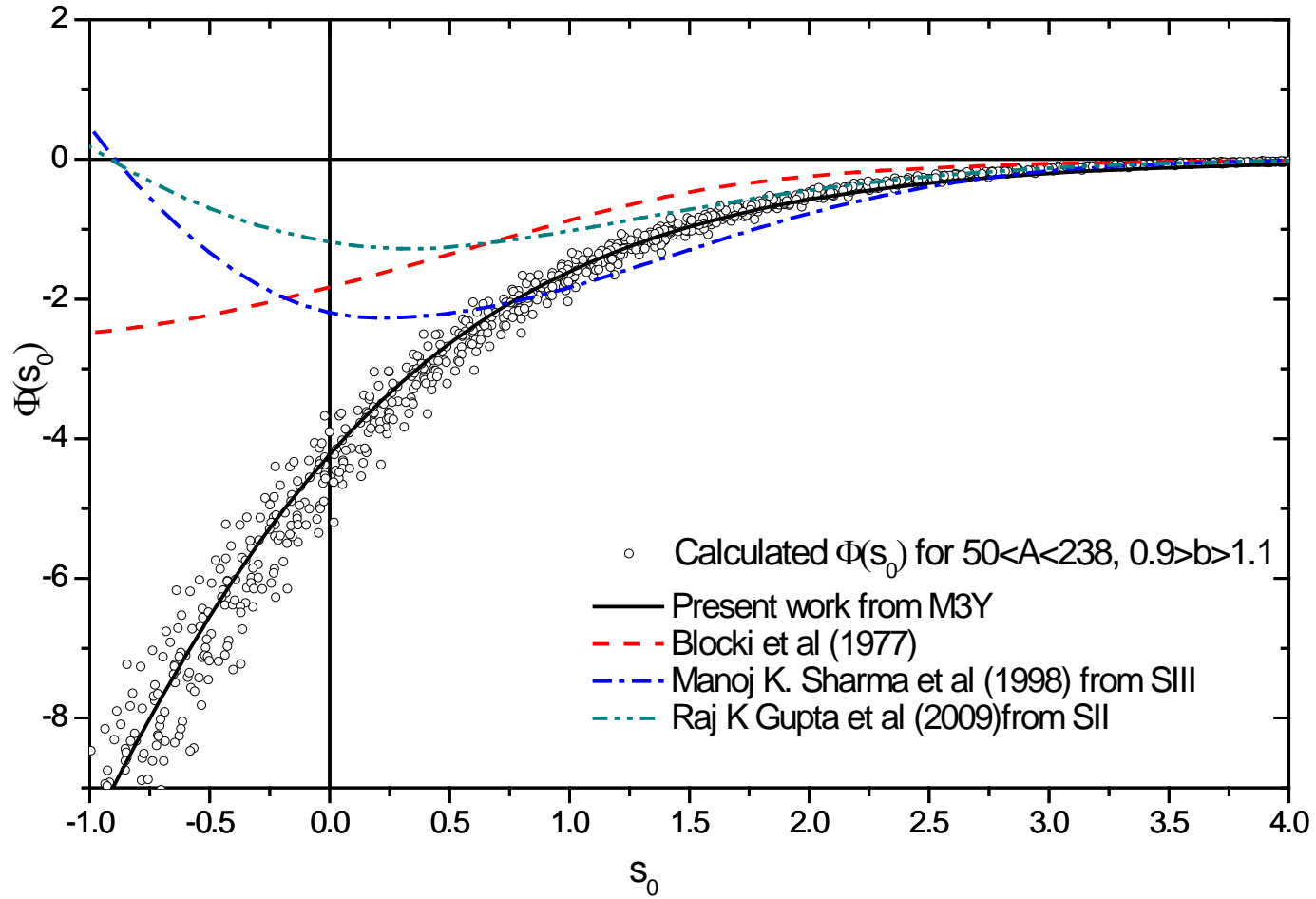


Figure (2.3-*b*) The same as Figure (2.3-*a*) but for reactions involve ions with mass numbers A as: $50 < A < 238$. Different shapes of the universal function are plotted [16, 24, 25].

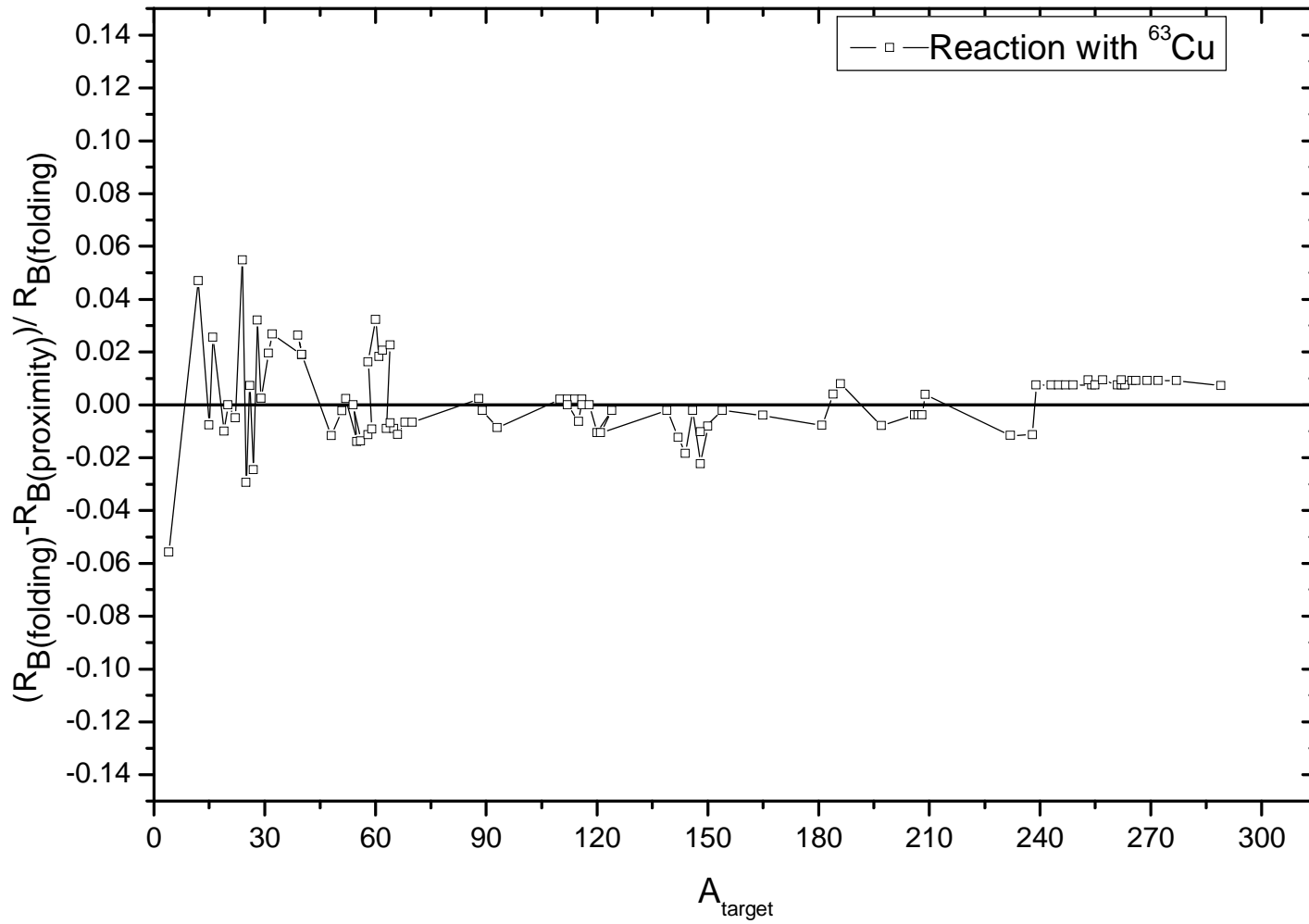


Figure (2.4-a) Fractional error between the values of potential barrier position calculated using the proximity model with universal function given by formula (2.9), and values calculated using DFM, for reactions between ^{63}Cu and different ions.

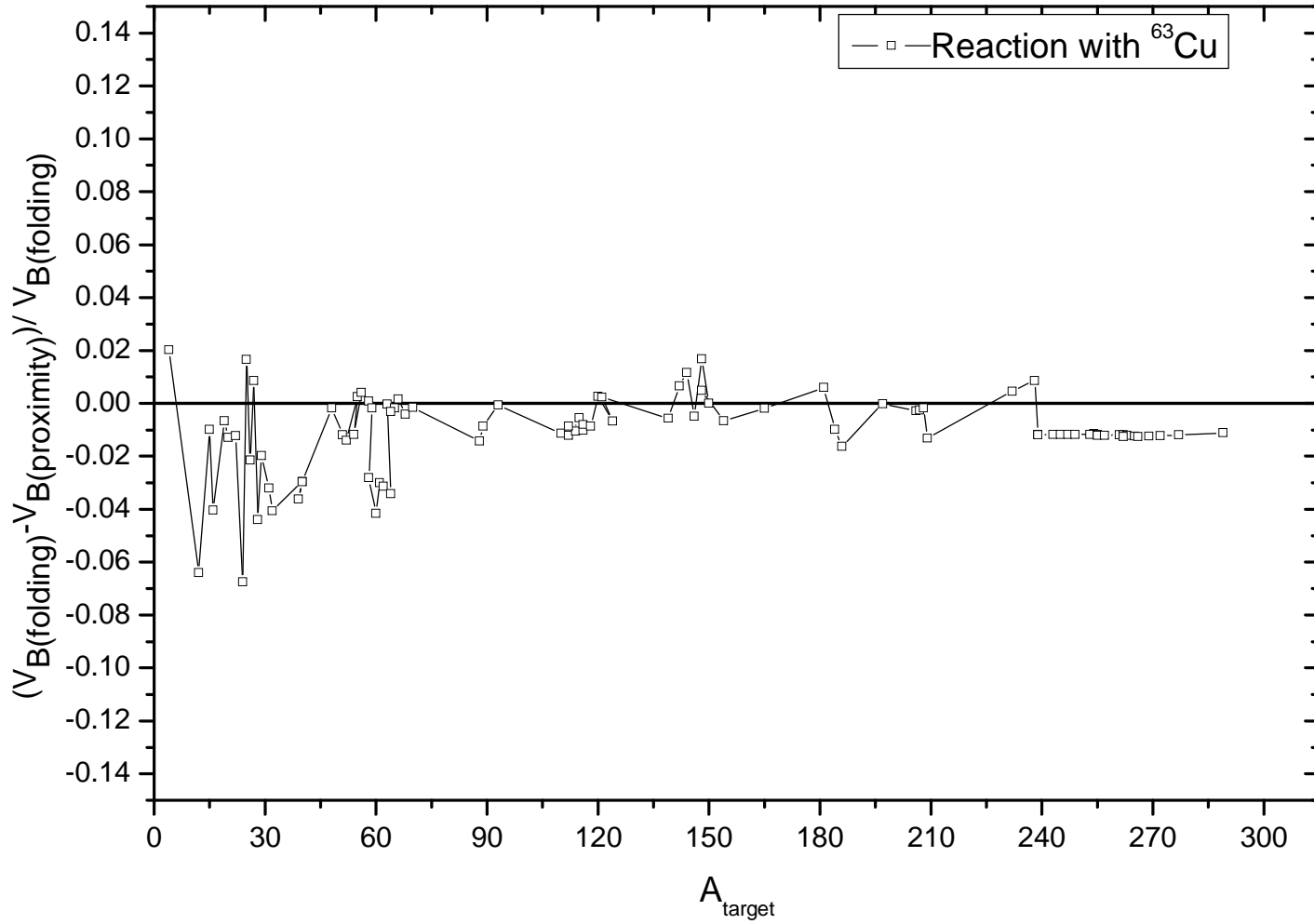


Figure (2.4-b) Fractional error between the values of potential barrier height calculated using the proximity model with universal function given by formula (2.9), and values calculated using DFM, for reactions between ^{63}Cu and different ions.

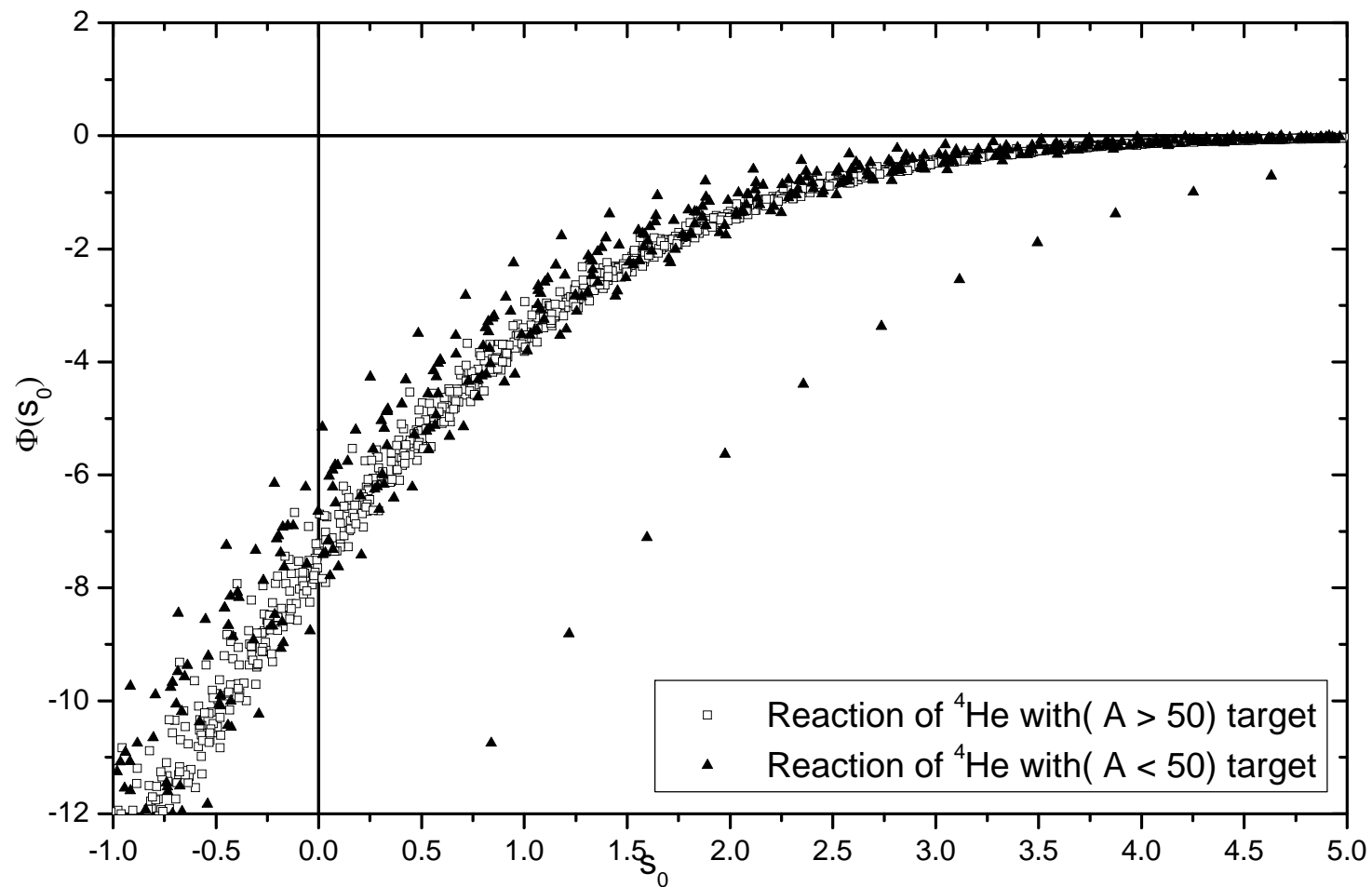


Figure (2.5-a) Calculated universal function $\Phi(s_0)$ as a function of the dimensionless separation s_0 , for reactions between ${}^4\text{He}$ and target nuclei with mass numbers up to 238.

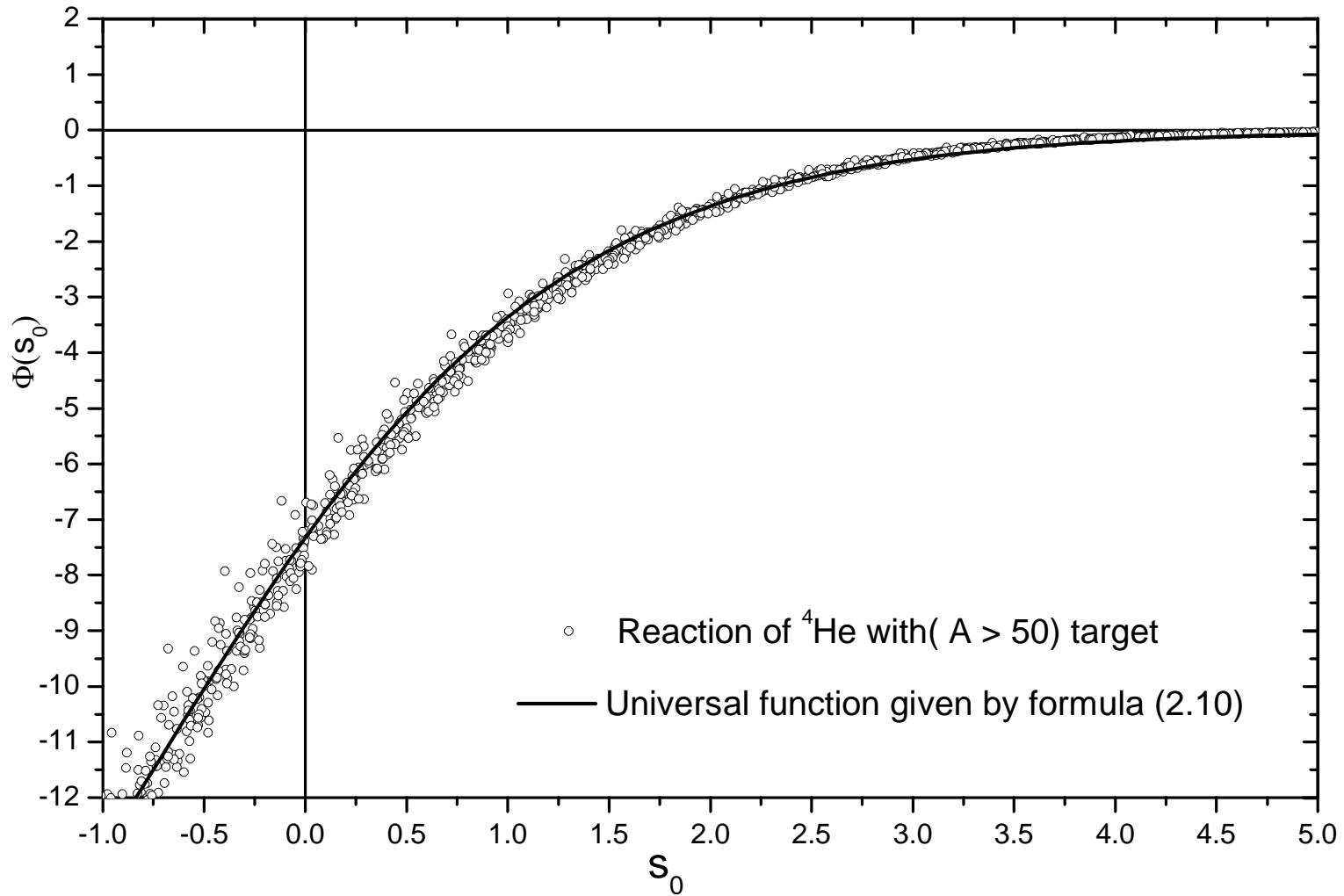


Figure (2.6-*b*) Same as Figure (2.5-*a*), but for target nuclei of mass numbers A as, $50 > A > 238$. The solid line is the universal function derived from the best fit to data, given by formula (2.10).

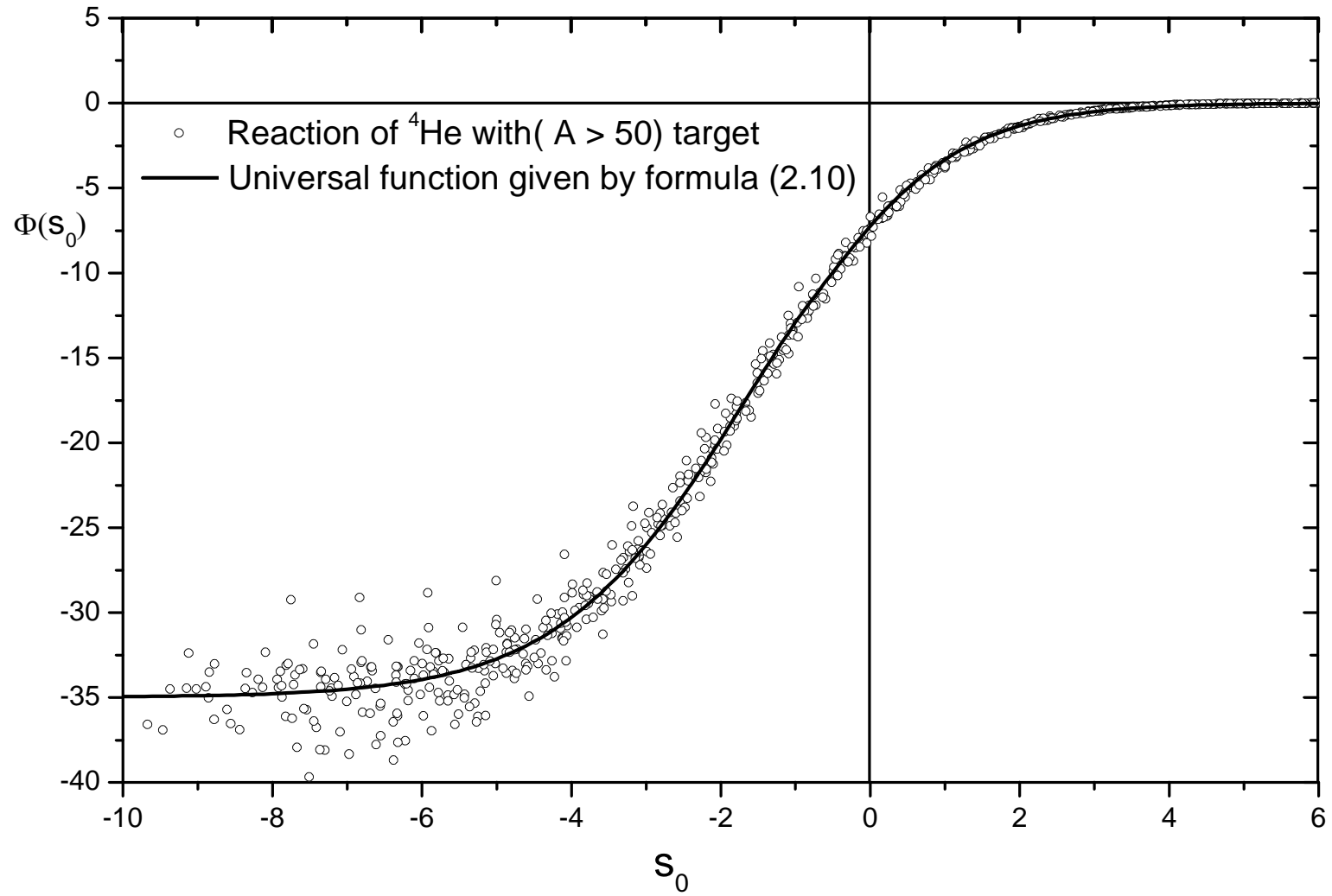


Figure (2.5-c) Same as Figure (2.5-b), but s_0 range varying in the range $[-10,6]$

2.3 Discussion

In the present chapter we use a method to derive a realistic universal function of proximity approach starting from realistic NN potential and nuclear density. For this purpose, we study only, the reactions involving ions which have density distributions given by the empirical formulae [28] listed in table (1.1). The idea of universality tells us that the values of the calculated universal function for all interactions must be sharply localized around an average line as a function of s_0 . From the calculations done in the present chapter, it is found that some ions like 4He and ${}^{60}Ni$ are far from the average $\Phi(s_0)$ line. Both the target and the projectile affect the value of the calculated universal function and the final result shows the average effect of the reaction pair. For example, considering an ideal symmetric pair, that gives exactly the average $\Phi(s_0)$ with no deviation, if one ion of this pair is replaced by another ion which causes an increase/decrease in the calculated universal function, the obtained line will be above/ below the average line. Moreover, if each of interacting ions leads to rising/lowering in the calculated universal function, the obtained universal function line will be more raised/ lowered. On this basis, symmetric reaction enhances the effect of any nucleus on the calculated universal function, because the reaction

partners have exactly the same effect. We consider the results of $\Phi(s_0)$ derived from 70 interacting pair. The results involved here are for symmetric reactions only, starting from ${}^4\text{He}-{}^4\text{He}$ up to ${}^{238}\text{U}-{}^{238}\text{U}$. The studied 70 reactions can efficiently give a complete picture of the possible 2485 reactions occurring between different isotopes in the range of study. It is worth mentioning that the main objective of the present work is to study the fusion barrier, and then we will give more attention to the data points around the barrier position ($-1 < s_0 < 5$).

In figure (2.2-*a*) the universal function $\Phi(s_0)$ calculated from M3Y interaction is plotted as a function of the dimensionless separation s_0 , for symmetric reactions between ions of mass numbers up to 238. It is obvious that the dispersion of different sets of data points increases as s_0 become more negative. The proximity model gives average estimate of the nuclear potential considering the surface to surface gap and the surface energy density. The DFM, unlike the proximity model, gives an average over all interactions, and the surface effect is automatically involved in the folded potential. For positive separations, largest contribution of the folding potential comes from surface interaction, and $\Phi(s_0)$, which stems from surface interaction, tends to be the same for all reactions.

In figure (2.2-b), the values of $\Phi(s_0)$ is plotted around the touching point and up to values which expected to be around the barrier positions. This figure shows that the data points for reactions involving nuclei of mass numbers less than 50 are more scattered than the rest of studied reactions. The spread of points in figure (2.2-b) indicates that it is impossible to get reasonable average universal function from M3Y NN force all over the range of the potential. The reaction between two ${}^4\text{He}$ nuclei has diffuseness (b) of 0.587 fm . while other reactions have diffuseness (b) around 1 fm . Moreover, ${}^4\text{He}$ nucleus has central nuclear density of $0.4229\text{ nucleon.fm}^{-3}$, while the rest of nuclei have central nuclear density of about $0.17\text{ nucleon.fm}^{-3}$. And it is also obvious the odd result for the reactions involving ${}^4\text{He}$, this is must be considered as a special case because of the unique nature of ${}^4\text{He}$. The reactions between ${}^4\text{He}$ projectile and other nuclei will be discussed separately later in this section.

Data included in figure (2.3-a, b) are for reactions with diffuseness (b) has values between 0.9 fm and 1.1 fm , and other reactions are excluded. It is found that some reactions which have smaller or higher values of b may increase the scattering of data points, for example, ${}^{60}\text{Ni} - {}^{60}\text{Ni}$ reaction has diffuseness $b = 0.842\text{ fm}$, and at $s_0 = 0$, $\Phi(s_0)$ is higher by about 0.5 from the

nearest data point for all pairs including ions of mass numbers as $50 \leq A \leq 238$. It is worth mentioning that there is only little number of nuclei which excluded; however, these nuclei will give more accurate results for their reactions with other nuclei.

The universal function of proximity is expected -from the original definition of proximity model- to be diffuseness independent, but the effect observed here is coming from the bulk nuclear reactions and not the surface-surface interaction. The nucleus is not sharp edged, but it has a diffused surface, so the half density radius -in some models- is taken to be the radius of the nucleus; and then there are a number of nucleons beyond the radius of the nucleus. In a given reaction between two nuclei, at $s_0 = 0$, the nucleons in the tail (nucleons beyond the radius of the nucleus) of each nucleus are completely inside the other, and the value of potential must be lower than calculated considering only the surface effect. Considering this idea, it is expected that reactions with higher diffuseness must have more negative $\Phi(s_0)$ at the same separations. The most of nuclei have diffuseness parameters within a small range around an average value, which make the differences due to tail nucleons overlap tend to be the same. It is clear from figure (2.3-*b*) that the values of the universal function at zero s_0 , spread

around -4.5 within a range of about 1.8, and the spread of data around an average value decreases as s_0 increases. So, it is impossible to state a formula for the universal function as a function of just one variable s_0 with accuracy higher than a certain limit. Inserting other parameters, such as the diffuseness parameter, into the universal function may improve the accuracy of the analytical formula produced, but in this case the name “universal” become no longer suitable for the new function, because it will lose its greatest property which is its universality.

The analytical formula of the universal function suitable for the present work has two main properties, the first: it has its greatest accuracy around the barrier position; the second: it must be a function of one variable s_0 . In other words, we have to give up some of accuracy to keep the universality of the universal function. This formula can be obtained from the best fit to the data around the barrier position. For this purpose we fit all the data points for s_0 larger than -1 in figure (2.3-b), the least square fit gives

$$\Phi(s_0) = \frac{-30}{1 + e^{\frac{s_0+1.57}{0.92}}}, \quad s_0 > -1.0 \quad (2.9)$$

This formula can easily be used in equation (2.1) to give the nuclear interaction between two heavy ions, then adding the Coulomb potential we obtain the Coulomb barrier. Different shapes of universal function [16, 24, 25] are plotted in figure (2.3-*b*), the common feature between the universal functions derived in these references is the presence of a hard core, this effect can appear if we only consider the surface effects as in reference [16], or if the universal function is derived from a potential having the same shape. The universal function introduced in the present chapter does not contain a hard core like that obtained from Skyrme forces [24, 25], but it has the same shape as the M3Y nucleus-nucleus potential. To test the ability of formula (2.9) in producing the parameters of the Coulomb barrier, we chose the reactions of ^{63}Cu as a fixed reactant with all ions given in table (1.1) beside its reactions with the trans-uranium elements with densities parameterized as presented in chapter (1). Figures (2.4-*a*, *b*) show the relative deviations between the results of DFM and the results derived from equation (2.9) for barrier position (R_B) and barrier height (V_B) respectively. In both figures, the reactions with light nuclei show large deviations, but for heavy and super heavy ions the deviations never exceed the 2%. However the shape of the universal function given by equation (2.9) is useful for barrier calculation, it

can not give a complete description of the nuclear part of heavy ion interaction.

The calculated universal function for reactions involve 4He projectile is illustrated in figures (2.5), it is obvious that the data points are less scattered than in figures (2.3), this is because of presence of fixed projectile, i.e. the deviations of different data sets comes from the effect of only one nucleus (the target). Fitting data points around the barrier position gives a function similar to (2.9), but in this case the obtained function can describe the interaction between 4He and heavy ions. Presence of such a universal function for 4He potential is very important in the field of α -particle studies. Recently proximity approach have been used by many authors to study half life times of α -decay of heavy and super heavy ions assuming proximity approach for barrier penetration. The same approach has been used for α -potential inside the nucleus. Those studies require a well defined universal function for any separation distance (s_0). Averaging over the calculated $\Phi(s_0)$ for all data points can give a single analytical formula for $\Phi(s_0)$ for any s_0 , but this formula become inaccurate for barrier calculations. To keep the accuracy for any s_0 , we fitted data around the barrier position separately, then the best formulation of $\Phi(s_0)$ for the reaction between 4He and HI, is

$$\Phi_{He}(s_0) = \begin{cases} \frac{-30}{1 + e^{\frac{s_0+1.17}{1.1}}}, & s_0 \geq -0.943 \\ \frac{-35}{1 + e^{\frac{s_0+1.66}{1.25}}}, & s_0 \leq -0.943 \end{cases} \quad (2.10)$$

which is useful for barrier calculation and give approximate value of the universal function for any separation distance.

Formula (2.10) can be used to approximate the nuclear potential for the reaction between 4He and HI of mass numbers between 50 and 238.

References

- [1] Yu.Ts. Oganessian, V.K. Utyonkov, Yu.V. Lobanov, et al., Phys. Rev. C 70 (2004) 064609.
- [2] V.Yu. Denisov and N.A. Pilipenko, Phys. Rev.C 76 (2007) 014602.
- [3] Monika Manhas and Raj K. Gupta, Phys. Rev. C 72 (2005) 024606 .
- [4] L.C. Chamon, G.P.A. Nobre, D. Pereira, E.S. Rossi, Jr., and C. P. Silva, Phys. Rev. C70 (2004) 014604.
- [5] M. Ismail, W.M. Seif, M.M. Osman, H. El-Gebaly, and N.M. Hassan, Phys. Rev. C 72 (2005) 064616.
- [6] L.C. Chamon, G. P.A.Nobre, D. Pereira, E. S. Rossi, C. P. Silva, L. R. Gasques, and B. V. Carlson, *ibid.* 70 (2004) 014604.
- [7] L.C. Chamon, B.V. Carlson, L.R. Gasques, D. Pereira, C. De Conti, M.A.G. Alvarez, M.S. Hussein M.A. Candido Ribeiro, E.S. Rossi, and C.P. Silva, Phys. Rev. C 66 (2002) 014610.
- [8] V. Yu. Denisov, Phys. Lett. B526 (2002) 315.
- [9] V.Yu. Denisov and W. Norenberg, Eur. Phys. J.A 15 (2002) 375.
- [10] S. Misticu and W. Greiner, Phys. Rev. C 66, 044606 (2002).
- [11] A. Iwamoto, P. Moller, J.R. Nix, and H. Sagawa, Nucl. Phys. A596 (1996) 329.
- [12] P. Moller and A. Iwamoto, Nucl. Phys. A575 (1994) 381.
- [13] M. Seiwert, W. Greiner, V. Oberacker, and M.J. Rhoades-Brown, Phys.Rev. C 29 (1984) 477.
- [14] G.R. Satchler, Direct Nuclear Reactions (Oxford Univ. Press, Oxford, 1983).

- [15] A. J. Baltz and B. F. Bayman, Phys. Rev. C 26 (1982)1969.
- [16] J. Blocki, J. Randrup, W. J. Swiatecki, and C. F. Tsang, Ann. Phys. (NY) 105 (1977) 427.
- [17] Raj K. Gupta, Dalip Singh, Raj Kumar and Walter Greiner, J. Phys. G: Nucl. Part. Phys. 36 (2009) 075104.
- [18] Raj K. Gupta, Narinder Singh, and Monika Manhas, Phys. Rev.C 70 (2004) 034608.
- [19] N. Malhotra and R. K. Gupta, Phys. Rev. C 31 (1985) 1179.
- [20] M.E. Brandan, G.R. Satchler, Phys.Rep. 285 (1997) 143.
- [21] M. Ismail, M. Osman, H. El-Gibaly, and A. Faessler, J. Phys. G: Nucl. Part. Phys. 15 (1989) 1291
- [22] A. Faessler, W. H. Dickhoff and M. Trefz, Nucl. Phys. A 428 (1984) 271.
- [23] T. Izumoto, S. Krewald, and A. Faessler, Nucl.Phys. A 341 (1980) 319.
- [24] Raj K. Gupta, Dalip Singh, Raj Kumar and Walter Greiner, J. Phys. G: Nucl. Part. Phys. 36 (2009) 075104.
- [25] Manoj K. Sharma, Rajeev K. Puri, Raj K. Gupta, Eur. Phys. J A 2 (1998) 69.
- [26] G. Bertsch, J. Borysowicz, H. McManus and W.G. Love, Nucl. Phys. A 284 (1977) 399.
- [27] R. Reid, Ann. Phys. 50 (1968) 411.
- [28] C.W. De Jager, H. De Vries, C. De Vries, Atomic Data And Nuclear Data Tables 14 (1974) 479.

Appendices

Appendix 1

DFM and Fourier transformation

The Fourier transform of a function $f(\mathbf{r})$ defined by

$$\tilde{f}(\mathbf{k}) = \int f(\mathbf{r}) e^{(i\mathbf{k}\cdot\mathbf{r})} d\mathbf{r}. \quad (\text{App. 1 - 1})$$

so that

$$f(\mathbf{r}) = (2\pi)^{-3} \int \tilde{f}(\mathbf{k}) e^{(-i\mathbf{k}\cdot\mathbf{r})} d\mathbf{k}. \quad (\text{App. 1 - 2})$$

The multipole expansion of the exponential term in (App.1-1) is given by

$$e^{(i\mathbf{k}\cdot\mathbf{r})} = 4\pi \sum_{l,m} i^l j_l(kr) Y_{lm}(\Omega_r) Y_{lm}^*(\Omega_k).$$

so that

$$\tilde{f}(\mathbf{k}) = 4\pi \sum_{l,m} i^l Y_{lm}^*(\Omega_k) \int j_l(kr) f(\mathbf{r}) r^2 d\mathbf{r} Y_{lm}(\Omega_r) d\Omega_r.$$

From the properties of spherical harmonics following

$$\int Y_{lm}(\Omega) d\Omega = \sqrt{4\pi} \delta_{l0} \delta_{m0}.$$

$$Y_{00}(\Omega) = \frac{1}{\sqrt{4\pi}}.$$

and if $f(\mathbf{r})$ in (App.1-1) is a scalar function of r and, then $\tilde{f}(k)$ has the form

$$\tilde{f}(k) = 4\pi \int j_0(kr) f(r) r^2 dr. \quad (\text{App. 1 - 3})$$

Similarly, the back Fourier transformation becomes

$$f(r) = 4\pi(2\pi)^{-3} \int j_0(kr) \tilde{f}(k) k^2 dk. \quad (\text{App. 1 - 4})$$

The expression of $\tilde{f}(k)$ given by (App.1-3) is very useful in the calculation of interaction potentials Fourier transform, as will be shown below.

Appendix 1-A: DFM in momentum space

The Fourier transform of the folded quantity is simply the product of the transforms of the individual component functions, as convolution theorem states. This makes the calculation much easier than directly doing the folding integrals. Making use of convolution theorem the DFM integral (App.1-3)

$$U(\mathbf{R}) = \int d\mathbf{r}_1 \int d\mathbf{r}_2 \rho_1(\mathbf{r}_1) v(\mathbf{r}_{12}) \rho_2(\mathbf{r}_2). \quad (\text{App. 1 - 5})$$

$$\tilde{U}(\mathbf{k}) = \tilde{\rho}_1(\mathbf{k}) \tilde{v}(\mathbf{k}) \tilde{\rho}_2(-\mathbf{k}). \quad (\text{App. 1 - 6})$$

If the nuclear density distribution $\rho_i(k)$ is spherically symmetric, we can apply the simplified expression (App.1-3) to get

$$\tilde{\rho}_i(k) = 4\pi \int j_0(kr) \rho_i(r) r^2 dr$$

So that

$$\begin{aligned} & \tilde{U}(\mathbf{k}) \\ &= \left[4\pi \int j_0(-kr_1) \rho_1(r_1) r_1^2 dr_1 \right] \tilde{v}(\mathbf{k}) \left[4\pi \int j_0(-kr_2) \rho_2(r_2) r_2^2 dr_2 \right] \end{aligned} \quad (\text{App. 1 - 7})$$

Applying (App.1-2) on the total potential

$$U(\mathbf{R}) = (2\pi)^{-3} \int \tilde{U}(\mathbf{k}) e^{(-i\mathbf{k}\cdot\mathbf{R})} d\mathbf{k}.$$

$\tilde{U}(\mathbf{k})$ is a scalar function as $\tilde{v}(\mathbf{k})$ is, then applying (App.1-4)

$$U(R) = 4\pi(2\pi)^{-3} \int k^2 J_0(kR) \tilde{U}(k) dk$$

$\tilde{U}(k)$ is defined in(App.1-7), then

$$U(R) = \left(\frac{1}{2\pi^2}\right) \int k^2 J_0(kR) \left[4\pi \int j_0(kr_1) \rho_1(r_1) r_1^2 dr_1\right] \tilde{v}(k) \left[4\pi \int j_0(-kr_2) \rho_2(r_2) r_2^2 dr_2\right] dk$$

which finally simplified to

$$U(R) = 8 \int k^2 J_0(kR) \tilde{v}(k) \left[\int j_0(kr_1) \rho_1(r_1) r_1^2 dr_1\right] \left[\int j_0(kr_2) \rho_2(r_2) r_2^2 dr_2\right] dk$$

(App. 1 – 8)

The expression of $U(R)$ given by (App.1- 8) is a powerful in the calculation of interaction potential between two spherical nuclei. Moreover, it is easy to calculate even numerically.

Appendix 1-B: Fourier transform of coulomb and M3Y potentials

B.1- Fourier transform of coulomb potentials

The coulomb potential between two protons of charge e and separated by distance r is

$$v_c(\mathbf{r}) = \frac{k_e e^2}{r}$$

Applying Fourier transformation given by (App.1- 3) for $v_c(r)$

$$\tilde{v}_c(k) = 4\pi k_e e^2 \int \frac{\sin(kr)}{kr} \frac{1}{r} r^2 dr$$

$$\tilde{v}_c(k) = \frac{4\pi k_e e^2}{k} \int \sin(kr) dr$$

replacing $\sin(kr)$ with its exponential form

$$\sin(x) = \frac{e^{ix} - e^{-ix}}{2i}$$

then we have

$$\tilde{v}_c(k) = \frac{4\pi k_e e^2}{k} \int \frac{e^{ikr} - e^{-ikr}}{2i} dr$$

making use of Yukawa trick

$$\tilde{v}_c(k) = \lim_{a \rightarrow 0} \frac{4\pi k_e e^2}{k} (e^{-ar}) \int \frac{e^{ikr} - e^{-ikr}}{2i} dr$$

$$\tilde{v}_c(k) = \lim_{a \rightarrow 0} \frac{4\pi k_e e^2}{k} \int \frac{e^{-(a-ik)r} - e^{-(a+ik)r}}{2i} dr$$

$$\tilde{v}_c(k) = \lim_{a \rightarrow 0} \frac{4\pi k_e e^2}{2ik} \left[\frac{e^{-(a-ik)r}}{-(a-ik)} + \frac{e^{-(a+ik)r}}{a+ik} \right]_0^\infty$$

$$\tilde{v}_c(k) = \lim_{a \rightarrow 0} \frac{4\pi k_e e^2}{2ik} \left[\frac{1}{(a-ik)} - \frac{1}{a+ik} \right]$$

$$\tilde{v}_c(k) = \frac{4\pi k_e e^2}{2ik} \left[\frac{2i}{k} \right]$$

so that, the coulomb potential in momentum-space is

$$\tilde{v}_c(k) = \frac{4\pi k_e e^2}{k^2} \quad (\text{App. 1 - 9})$$

B.2- Fourier transform of M3Y potentials

The first two terms of M3Y interaction potential have the shape of Yukawa potential which has the form of

$$v_Y(\mathbf{r}) = \frac{V_0 e^{-\alpha r}}{\alpha r}.$$

Applying Fourier transformation given by (App.1- 3) for $v(r)$

$$\tilde{v}_Y(k) = 4\pi \int \frac{\sin(kr)}{kr} \frac{V_0 e^{-\alpha r}}{\alpha r} r^2 dr$$

$$\tilde{v}(k) = 4\pi \frac{V_0}{k\alpha} \int \sin(kr) e^{-\alpha r} dr$$

replacing $\sin(kr)$ with its exponential form

$$\tilde{v}_Y(k) = \frac{4\pi V_0}{2ik\alpha} \int e^{(ik-\alpha)r} - e^{-(ik+\alpha)r} dr$$

$$\tilde{v}_Y(k) = \frac{4\pi V_0}{2ik\alpha} \left[\frac{e^{-(ik-\alpha)r}}{ik-\alpha} + \frac{e^{-(ik+\alpha)r}}{ik+\alpha} \right]_0^\infty$$

$$\tilde{v}_Y(k) = \frac{4\pi V_0}{2ik\alpha} \left[\frac{1}{-ik + \alpha} - \frac{1}{ik + \alpha} \right]$$

$$\tilde{v}_Y(k) = \frac{4\pi V_0}{2ik\alpha} \left[\frac{ik + \alpha + ik - \alpha}{k^2 + \alpha^2} \right]$$

$$\tilde{v}_Y(k) = \frac{4\pi V_0}{2ik\alpha} \left[\frac{2ik}{k^2 + \alpha^2} \right]$$

$$\tilde{v}_Y(k) = \frac{4\pi V_0}{\alpha[k^2 + \alpha^2]} \quad (\text{App. 1 - 10})$$

The exchange term in M3Y potential has the form of delta shape potential of the form

$$v_D(\mathbf{r}) = V_0 \delta(\mathbf{r})$$

using the integral

$$\int e^{(-ik \cdot \mathbf{r})} d\mathbf{k} = (2\pi)^3 \delta(\mathbf{r})$$

and comparing with the expression of Fourier transformation (App.1-2), therefore, the function ($f(\mathbf{k}) = 1$) is the Fourier transform of ($f(\mathbf{r}) = \delta(\mathbf{r})$), and the exchange term in momentum space becomes

$$\tilde{v}_D(k) = V_0 \quad (\text{App. 1 - 11})$$

M3Y potential that used in this work has the shape of

$$v_n(r) = \frac{7999 e^{-4r}}{4r} - \frac{2134 e^{-2.5r}}{2.5r} - 262\delta(r)$$

Making use of (App.1-10) and (App.1-11), so that, the M3Y potential in momentum-space is

$$\tilde{v}_n(k) = \frac{7999 \times 4\pi}{4[k^2 + 4^2]} - \frac{2134 \times 4\pi}{2.5[k^2 + 2.5^2]} - 262 \quad (\text{App. 1 - 12})$$

Appendix 2

Units of Coulomb constant

The coulomb potential between two protons of charge e and separated by distance r is

$$v_c(\mathbf{r}) = \frac{k_e e^2}{r}$$

and

$$k_e = \frac{1}{4\pi\epsilon_0}$$

where the constant ϵ_0 is the *permittivity of free space* and has the value $8.8542 * 10^{-12} \text{F/m}$, and $e = 1.60219 * 10^{-19}$ is the charge of proton. So that, the potential obtained using these constants, with there SI units, is in Joules when the distance is in meters.

If the *fm* is used as a unit of r the permittivity of free space convert to

$$\epsilon_0 = 8.854 2 * 10^{-27} \text{ F/fm.}$$

and the potential convert to be in MeV as

$$v_c(r) = \left(\frac{1}{4\pi\epsilon_0} \frac{e^2}{r} \right) \left(\frac{10^{-6}}{e} \right) \text{ MeV}$$

then, the Coulomb potential is given in MeV ,when r is given in fm, by

$$v_c(r) = (1.439 974 579) \left(\frac{1}{r} \right) \text{ MeV} \quad (\text{App. 2 - 1})$$

المستخلص

في الفصل الاول تم حساب بارامترات حاجز الجهد (مكان الحاجز وارتفاعه) لعدد كبير من أزواج الأنوية المختلفة باستخدام نموذج الطى المزدوج، بدءاً من دالة واقعية لتوزيع المادة النووية داخل الأنوية. وتمت دراسة سلوك بارامترات حاجز الجهد مع أعداد الكتلة، والشحنات، و أنصاف أقطار الأنوية المتفاعلة. تم تقديم السلوك المنتظم لبارامترات حاجز الجهد في صورة صيغ تحليلية بسيطة، يمكن استخدامها لحساب مكان وارتفاع حاجز الجهد مباشرة، كما تظهر العوامل التي يمكن أن تؤثر عليها.

في الفصل الثاني تم استخدام قيم الجهد الناتجة من حسابات نموذج الطى المزدوج لاستنتاج دالة عامة للتقارب النووي (universal function of nuclear proximity) يمكن استخدامها لحساب الجهد بين نواتين حول حاجز الجهد. كما تم استخدام الدالة الجديدة لحساب بارامترات حاجز الجهد ووجد ان الفرق بينها وبين القيم المحسوبة باستخدام نموذج الطى المزدوج لا تتجاوز (2%) لكل الأنوية الثقيلة والفائقة الثقل. كما تم تقديم دالة مماثلة لحساب الجهد بين الأنوية الثقيلة و جسيمات الفا.

دراسة بارامترات حاجز الجهد بين أزواج الأنوية
المختلفة

إعداد

عبدالغنى رضا عبدالغنى أحمد

رسالة مقدمة إلي
كلية العلوم

كجزء من متطلبات الحصول علي درجة
الماجستير في العلوم
(فيزياء نظرية)

قسم الفيزياء
كلية العلوم
جامعة القاهرة
(٢٠١٠)